NUMERICAL ANALYSIS OF STRUCTURAL MASONRY

By

REZA USHAKSARAEI, B. ENG., M. ENG.

A Thesis

Submitted to the School of Graduate Studies

in Partial Fulfilment of the Requirements

for the Degree

Doctor of Philosophy.

McMaster University

DOCTOR OF PHILOSOPHY (2002)	**McMaster University**
(Civil Engineering)	**Hamilton, Ontario,**
	Canada

TITLE: **NUMERICAL ANALYSIS OF STRUCTURAL MASONRY**

AUTHOR: **Reza Ushaksaraei**

B. Eng., M. Eng. (Tehran University, Tehran, Iran)

SUPERVISOR: **Dr. S. Pietruszczak**

NUMBER OF PAGES: **xii, 95**

ABSTRACT

This thesis presents a comprehensive approach to numerical modelling of the nonlinear behaviour of structural masonry. Masonry is a heterogenous material, which displays orthotropic symmetry. The anisotropy effects are described here by incorporating a set of distribution functions specifying the directional dependence of material properties.

In the first part, a macroscopic failure criterion for structural masonry is proposed. This criterion is derived within the framework of the critical plane approach. First, a general discussion is provided examining the performance of this framework within the context of both classical linear and nonlinear criteria. Subsequently, a bi-linear form of failure criterion for structural masonry is proposed. Extensive numerical study is performed examining the behaviour in biaxial compression-tension and compression-compression regimes for different orientations of the sample relative to the loading direction. The results are compared with the available experimental data.

In the next part, the results of a 3D seismic analysis of the masonry walls of a power substation building - typical of those constructed in the Montreal region in Canada - are presented. The analysis is conducted in the elastic range, assuming orthotropic material properties, and the admissibility of the stress field is assessed based

on the proposed failure criterion. A numerical study is performed examining the effect of different reinforcement strategies.

The focus of the last part of this thesis is on the description of progressive failure in structural masonry. A continuum formulation is developed here which is applicable to a representative volume comprised of a large number of units interspersed by mortar joints. The framework defining the conditions at failure when employing the critical plane approach is extended to model the inelastic deformation process. This is accomplished by incorporating a multi-laminate approach in which the average response is derived from sliding/separation characteristics along a set of randomly distributed planes. The localized deformation is described by considering a structured medium comprising the intact masonry intercepted by a distinct macrocrack. Extensive numerical simulations are performed examining the response of brickwork in compression/tension regimes at different orientations of the bed joints relative to the loading direction. A boundary-value problem which involves an inelastic finite element analysis of a bearing masonry wall subjected to in-plane loading is also studied.

ACKNOWLEDGMENTS

I would like to express my sincere appreciation to my supervisor, Dr. Stan Pietruszczak, for his valuable guidance, encouragement, and effective supervision during every stage of this research work. No words can express my gratitude for his excellent supervision.

The valuable comments of Dr. Dieter Stolle and Dr. Mateusz Sklad, members of the supervisory committee, are also greatly appreciated.

I would like to acknowledge the financial support of the Department of Civil Engineering at McMaster. I am also grateful to the Government of Ontario for the financial support through the Ontario Graduate Scholarship.

I would like to thank my wife, Roza, and my son, Alireza, for their understanding and continuous encouragement. Finally, I would like to dedicate this thesis to the memory of my beloved mother, Maryam. Without her dedications, I would have never reached this stage in life.

TABLE OF CONTENTS

LIST OF FIGURES

CHAPTER 1

INTRODUCTION

Masonry has been the most broadly used material since the beginning of human history. Despite its popularity, there is no rigorous approach for the analysis of masonry structures, which is primarily due to the heterogeneity and nonlinearity of the material. The need for a reliable assessment of mechanical properties and specification of the conditions at failure has motivated the work of many researchers. In section 1.1 a literature review is presented. It is clear from this review that no rigorous constitutive model for structural masonry exists, which would be suitable for incorporation in a nonlinear finite element analysis. This aspect was the main motivation for the present research. Section 1.2 describes the outline of the research and includes a brief discussion and the objectives of each chapter.

1.1 Literature Review

One of the main components of research in structural masonry is that involving the experimental investigation of the behaviour of brickwork. The tests are typically conducted on masonry panels subjected to biaxial compression/tension at different orientation of the bed joints relative to the loading direction. For example, Samarasinghe and Hendry (1982) performed a series of tests on one-sixth scale brickwork under uniform biaxial tensile and compressive stresses. They derived the equation of a failure surface relating the principal stresses at failure to the angle of inclination of the bed joints for the compression-tension case. Page (1983) performed a series of biaxial tension-compression tests on one-half brickwork to define a 3D failure surface. The two previous works are conceptually the same. However, the latter seems to provide the most comprehensive experimental data available so far. In an earlier work, Page (1981) presented the results of the tests on half-scale brickwork, for biaxial compressive strength of brick masonry. Drysdale and Khattab (1995) investigated experimentally the behaviour of grouted concrete masonry under biaxial tension-compression loading conditions. Modes of failure, strength parameters and the deformation characteristics were found to depend on the bed joint orientation and the principal stress ratio. The specimens were built using full-size hollow concrete blocks. The results of experimental data have provided valuable information used to establish empirically or semi-empirically based methodologies for the design of masonry structures.

Another aspect of masonry research is related to the description of mechanical properties of brickwork. In general, the numerical analysis of large masonry structures, such as arch bridges, historic monuments, etc., cannot be conducted on the basis of examining individual brick units. Therefore, some macroscopic formulations should be employed which are capable of describing the anisotropic properties of the brickwork. In this context, a representative element of brickwork may be regarded as a structured medium comprising the brick units interspersed by sets of continuous bed joints and discontinuous head joints. In recent years, several attempts have been made to estimate the average properties of masonry panels. Those include micropolar Cosserat continuum models (e.g., Sulem & Muhlhaus, 1997; Masiani & Trovalusci, 1996) as well as applications of the mathematical theories of homogenization for periodic media (e.g., Anthoine, 1995, 1997; Urbanski et al., 1995). Such approaches, although rigorous, have never been implemented in the context of a structural analysis of practical engineering problems. For Cosserat media, one of the main difficulties is the development of a systematic methodology for identification of equivalent continuum properties. For a rigorous homogenization approach, the extension to inelastic range poses profound conceptual problems and is not, in general, feasible. For instance, in the approach pursued by Anthoine (1995, 1997), the solution at the level of a basic cell was obtained numerically by employing the finite element technique. Subsequently, a linear elastic operator was established relating the average macroscopic strain and stress tensors. Although the approach is quite accurate, it cannot, in general, be implemented in the inelastic range.

Given these difficulties, a number of simplified approaches have been developed incorporating various idealizations at the level of either the geometry of brickwork or the interaction between the constituents. Such approximate homogenization techniques include the works of Pande et al. (1989), Maier et al. (1991), Lourenco & Zucchini (2001), etc. For example, Pande et al. (1989) presented an 'equivalent' material approach for the computation of the elastic properties of the masonry. A stacked brick-mortar system consisting of a series of parallel layers which behaved elastically was introduced. This was extended such that masonry with two sets of bed and head mortar joints could be represented by an equivalent homogenous orthorhombic elastic material. Expressions for the elastic properties of the equivalent material were derived in terms of the elastic properties of the brick and mortar together with relative thickness. Even for these simplified models, however, the implementation in the context of a non-linear finite element analysis is still a difficult task and has not yet been accomplished.

The research involving numerical analysis of real masonry structures is rather restrictive. There have been, however, several attempts reported in the literature. For instance, Lemos (2001) presented a numerical modelling study of a stone masonry arch and pillar structure under a cyclic loading. The numerical model was based on a discrete element formulation with deformable (elastic) blocks; i.e., the blocks were discretised internally into a finite element mesh. The joints were assumed to follow an elasto-plastic model governed by a Coulomb slip criterion, assuming no cohesion, no tensile strength, and no dilation. The main disadvantage of this method stems from the fact that it cannot be computationally justified for structures comprising a large number of masonry units. Another example of the finite element analysis of structural masonry is a numerical modelling of masonry arch bridges by Sicilia et al. (2001). The authors presented a three-dimensional finite element model, which used a homogenization technique to simulate the complex behaviour of masonry and the interfaces within the structure. The model was then used to simulate the results of a centrifuge test of Pontypridd Bridge. In order to consider the anisotropy of masonry and its complex failure mechanisms in the model with a limited computational cost, a two-step homogenization technique (Pande et al., 1989) was used; assuming the elastic behaviour for the material. The procedure was based on an averaging rule for stresses and strains and a series of hypotheses for the unit-mortar bond. The failure criterion considered was Mohr-Coulomb with tension cut-off for each constituent plus additional shear and tensile checks in the specific orientation of the bed and head joints. Once failure was detected in either of the constituents, a crack in the appropriate orientation was generated and smeared in a further step of homogenization. In order to provide a simulation with a limited computational cost, the behaviour of interfaces was approximated using an equivalent element spanning over the materials involved and defined based on the homogenization technique employed to simulate masonry (Pande and Lee, 1992). The numerical results were not in very good agreement with the experimental data reported by the authors in the same reference. For instance, the numerical model underestimated the movements of the arch between the load and the crown; and in the final loading stages, the final decrease in stiffness recorded in the centrifuge test could not be reproduced numerically. There are other examples of finite element analysis reported in the literature. However, all of these attempts suffer from the lack of a rigorous modelling of the behaviour of structural masonry in both elastic and inelastic range.

1.2 Outline of the Research

As mentioned previously, introducing a reliable description of mechanical properties of masonry is vital to ensure the accuracy of the results of a finite element analysis. Thus, the main objective of this research is to formulate a constitutive model for structural masonry, which is not only simple, but also can reflect the basic trends in the physical behaviour of the material. In particular, the model proposed in this research can properly predict the orientation of the failure plane, which is of significant importance for defining the post-localization response of the material. Furthermore, when analysing a masonry structure, the evolution of the pattern of cracks can be monitored, which can provide insight into the global response of the structure leading one to choose an efficient reinforcing strategy. In what follows, a general discussion on each individual chapter is presented, outlining the scope of the research.

In chapter 2, a failure criterion for structural masonry is presented (Ushaksaraei and Pietruszczak, 2002). The approach involves, in essence, an extension of non-linear Coulomb failure theory for the case of anisotropy, as implied by the geometric arrangement of the brickwork.

In the past, several attempts have been made to modify the Mohr-Coulomb criterion for geomaterials, such as overconsolidated clays or sedimentary rocks, which display strong anisotropic properties. The first attempt was made, on an empirical basis, by Casagrande and Carrillo (1944). The authors considered the two simplest cases involving an anisotropic purely cohesive and cohesionless soils, with the further restraint that the intermediate principal stress was in the plane of material isotropy. Both graphical and analytical solutions were given for the shear strength and the location of the failure plane. Later, further modifications were proposed by other researchers. For instance, Jaeger (1960) introduced a model, known as 'the single plane of weakness theory,' which was based on a simple generalization of the Coulomb criterion for the shear failure of anisotropic rocks. Later, Hoek and Brown (1980) developed an empirical relationship between the principal stresses at failure which incorporated an analogy with the nonlinear failure envelope predicted by classical Griffith crack theory for plane compression (Hoek, 1968). A comprehensive review of various approaches is provided in the article by Duveau et al. (1998).

The methodology adopted here is based on incorporating a critical plane approach as developed by Pietruszczak and Mroz (2001). This approach involves the notion of the existence of a critical plane, or the localization plane, on which the failure function, expressed in terms of normal and tangential components of the traction vector, reaches a maximum. Chapter 2 is written in the following sequence. In section 2.1, an extension of the critical plane framework is presented for the case of a non-linear failure function, which is more suitable for the class of brittle materials, such as rocks or masonry. Subsequently, a macroscopic failure criterion for structural masonry is proposed which incorporates a bi-linear approximation of the quadratic form employed in section 2.1. In section 2.3, an extensive numerical analysis is carried out. First, the question of identification of material functions/parameters is addressed in relation to experimental data reported by Page (1983). Later, the formulation is applied to examine the conditions at failure in a brickwork panel. In particular, a series of biaxial compression-tension and compression-compression loading histories is examined for different orientations of the bed joints and the results are compared with the test data.

Chapter 3 is devoted to an application of the failure criterion proposed in chapter 2. In this chapter the results of the seismic analysis of brick walls of a power substation building, similar to Saraguay substation, located in the north-western part of the Montreal Island in Quebec, Canada, are presented (Gocevski et al., 2002). The main objective is the examination of the performance of the masonry walls of the substation under seismic excitation. The analysis is conducted in the elastic range assuming orthotropic material properties, estimated based on a homogenization procedure proposed by Pietruszczak and Niu (1992). The plastic admissibility of the resulting stress field is examined using the failure criterion proposed in chapter 2.

The main objective of chapter 4 is to develop a continuum theory for describing the inelastic behaviour of structural masonry. This approach may be perceived as a pragmatic alternative to the homogenization method. It is simpler in numerical implementation and addresses all stages of the deformation process, including the localized deformation associated with the formation of macrocracks. In section 4.1, a general formulation of the problem is provided. In section 4.1.1, a brief review of the conditions at failure, described by invoking a critical plane approach, is presented. This approach is subsequently extended to incorporate the inelastic deformation (section 4.1.2). This is accomplished by attributing the inelastic behaviour to sliding/separation along an infinite number of randomly oriented planes. The behaviour along each plane is defined in terms of a plasticity framework and the global macroscopic response is obtained by averaging the contributions from all active planes. Section 4.1.3 is devoted to the description of localized deformation. Here, the formation of macrocracks is perceived as a localization problem and the formulation is derived by incorporating a homogenization procedure which employs a 'characteristic dimension'. The general mathematical framework is illustrated by the numerical examples provided in section 4.2. Here, the details pertaining to the specification of material functions/parameters are discussed first (section 4.2.1), followed by numerical analyses examining the response of brickwork in compression and tensions regimes for different orientations of the bed joints. The chapter concludes with the results of a finite element analysis of a bearing masonry wall subjected to in-plane loading (section 4.3). Here, the evolution of the crack pattern is examined prior to the collapse of the wall.

CHAPTER 2

FAILURE CRITERION FOR STRUCTURAL MASONRY BASED ON CRITICAL PLANE APPROACH

In this chapter, a macroscopic failure criterion for structural masonry is presented (Ushaksaraei and Pietruszczak, 2002). This criterion is derived within the framework of the critical plane approach, which has recently been developed by Pietruszczak and Mroz (2001). In section 2.1, an extension of this framework is given for the case of a non-linear failure function, which is more suitable for the class of brittle materials, such as rocks or masonry. In section 2.2, a macroscopic failure criterion for structural masonry is proposed, which incorporates a bi-linear approximation of the quadratic form employed in section 2.1. In section 2.3, an extensive numerical analysis is carried out. First, the question of identification of material functions/parameters is addressed in relation to experimental data reported by Page (1983). Later, the formulation is applied to examine the conditions at failure in a brickwork panel. In particular, a series of biaxial compression-tension and compression-compression loading histories is examined for different orientations of the bed joints and the results are compared with the experimental data.

2.1 Critical Plane Approach; Extension to a Nonlinear Failure Criterion

The critical plane approach consists of specifying the orientation of a critical plane on which the failure function reaches a maximum. Consider the case of a failure function in a quadratic form

$$F = a\tau^2 + b\tau + \sigma - c = 0 \tag{2.1}$$

where τ and σ represent the shear and normal components of the traction vector on the plane with unit normal n_i. Thus,

$$\tau = \sigma_{ij} n_i s_j, \qquad \sigma = \sigma_{ij} n_i n_j \tag{2.2}$$

where

$$s_i = t_i^s / \| t_i^s \|, \qquad t_i^s = (\delta_{ij} - n_i n_j)\sigma_{jk} n_k \tag{2.3}$$

and t_i^s denotes the tangential component of the traction vector on this plane. In equation (2.1), the material parameters a, b and c are defined in terms of distribution functions

$$a = a_o(1 + \Omega_{ij}^a n_i n_j), \quad b = b_o(1 + \Omega_{ij}^b n_i n_j), \quad c = c_o(1 + \Omega_{ij}^c n_i n_j) \tag{2.4}$$

in which a_o, b_o and c_o are the respective orientation averages of a, b and c, whereas Ω's represent a set of symmetric traceless tensors which describe the bias in the directional distribution of these parameters. The orientation of the localization plane can be determined by maximizing the failure function F with respect to n_i and s_i, subject to the constraints

$$n_i n_i = 1, \; s_i s_i = 1, \; n_i s_i = 0 \tag{2.5}$$

Introducing Lagrange multipliers λ_1, λ_2, and λ_3, the corresponding Lagrangian function becomes

$$G = a_o(1 + \Omega^a_{jk}n_jn_k)(\sigma_{pq}n_ps_q)^2 + b_o(1 + \Omega^b_{jk}n_jn_k)(\sigma_{pq}n_ps_q) + \sigma_{jk}n_jn_k$$
$$- c_o(1 + \Omega^c_{jk}n_jn_k) - \lambda_1(n_jn_j - 1) - \lambda_2n_js_j - \lambda_3(s_js_j - 1) \tag{2.6}$$

The stationary conditions of G with respect to n_i and s_i yield a set of equations

$$\frac{\partial G}{\partial n_i} = 2a_0\Omega^a_{ij}n_j(\sigma_{pq}n_ps_q)^2 + 2a_0(1 + \Omega^a_{jk}n_jn_k)(\sigma_{pq}n_ps_q)(\sigma_{ir}s_r)$$
$$+ 2b_o\Omega^b_{ij}n_j(\sigma_{pq}n_ps_q) + b_o(1 + \Omega^b_{jk}n_jn_k)\sigma_{iq}s_q - 2c_0\Omega^c_{ij}n_j + 2\sigma_{ij}n_j - 2\lambda_1n_i - \lambda_2s_i = 0$$

$$\frac{\partial G}{\partial s_i} = 2a_0(1 + \Omega^a_{jk}n_jn_k)(\sigma_{pq}n_ps_q)(\sigma_{ir}n_r) + b_o(1 + \Omega^b_{jk}n_jn_k)(\sigma_{iq}n_q) - \lambda_2n_i - 2\lambda_3s_i = 0 \tag{2.7}$$

whereas the stationary conditions with respect to λ's provide the constraints (2.5). The resulting set of algebraic equations can be solved for both the direction cosines n_i and s_i, as well as the Lagrange multipliers. Given n_i and s_i, the criterion (2.1) can then be verified to determine whether the conditions at failure have been reached.

Given the representation (2.1), the standard *Coulomb* criterion can be obtained by setting $a_o = 0$. At the same time, by dropping the term involving σ and assuming $a_o = 0$, $b_o = 1$ and $\Omega^b_{ij} = 0$, the *Tresca* criterion is recovered. In the latter case, the Lagrangian function (2.6) becomes

$$G = \sigma_{jk}n_js_k - c_0(1 + \Omega^c_{jk}n_jn_k) - \lambda_1(n_jn_j - 1) - \lambda_2n_js_j - \lambda_3(s_js_j - 1) \tag{2.8}$$

so that the stationary conditions with respect to n_i and s_i yield the set of equations

$$\begin{aligned} \frac{\partial G}{\partial n_i} &= (\sigma_{ij} - \lambda_2 \delta_{ij}) s_j - 2(c_0 \Omega^c_{ij} + \lambda_1 \delta_{ij}) n_j = 0 \\ \frac{\partial G}{\partial s_i} &= (\sigma_{ij} - \lambda_2 \delta_{ij}) n_j - 2\lambda_3 s_i = 0 \end{aligned} \tag{2.9}$$

which together with (2.5) can be solved for n_i, s_i and λ's.

It should be noted that the maximazation problem (viz. eq. 2.7 or eq. 2.9), can be formulated in terms of fewer unknowns. In particular, the representation (2.3) can be substituted in the functional form of F, eq.(2.1), thereby leading to a Lagrangian function G which depends only on the unit vector n_i

$$\begin{aligned} G = {} & a_o (1 + \Omega^a_{jk} n_j n_k)(\delta_{pq} - n_p n_q)(\delta_{pm} - n_p n_m)\sigma_{qs}\sigma_{ml} n_s n_l \\ & + b_o (1 + \Omega^b_{jk} n_j n_k)\, [(\delta_{pq} - n_p n_q)(\delta_{pm} - n_p n_m)\sigma_{qs}\sigma_{ml} n_s n_l]^{\frac{1}{2}} \\ & + \sigma_{jk} n_j n_k - c_o (1 + \Omega^c_{jk} n_j n_k) - \lambda(n_j n_j - 1) \end{aligned} \tag{2.10}$$

It is evident that such an approach will reduce the number of simultaneous equations at the expense, however, of introducing higher degree terms in n_i. Thus, it will not, in general, be computationally more efficient.

In order to illustrate the framework outlined above, consider the sample of a transversely isotropic brittle-plastic material, such as a stratified rock, subjected to plane strain axial compression under a constant confining pressure $p_0 = -\sigma_1 = \text{const}$. The geometry of the problem is defined in figure 2.1. The sample is referred to a fixed frame of reference $\{x_1, x_2, x_3\}$, while the principal material triad is defined by the base vectors $e^{(1)}, e^{(2)}, e^{(3)}$. The direction of the major principal stress σ_2 is taken along the x_2-axis and the principal material direction $e^{(3)}$ is considered to coincide with the x_3 -axis. Furthermore, the angle β specifies the orientation of the bedding planes relative to the horizontal x_1-axis.

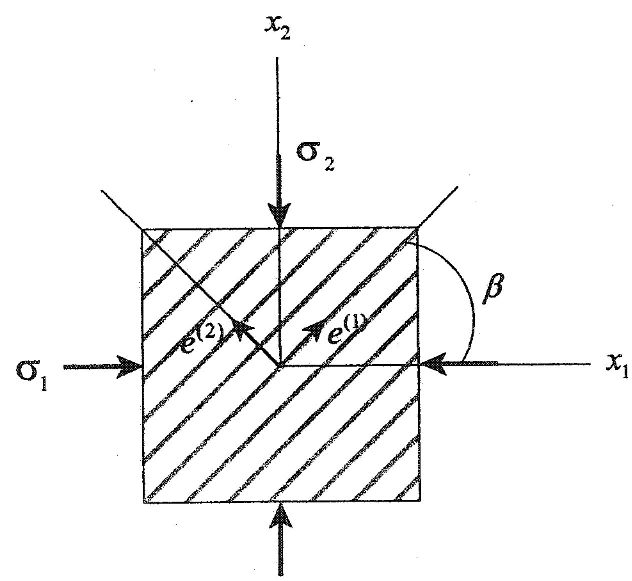

Figure 2.1 Geometry of the problem.

The results of the numerical simulations, employing the parabolic criterion (2.1), are shown in figures 2.2 to 2.5. The simulations have been performed assuming $b_0 = 0$, $a_0 = 0.04\ (\mathrm{MPa})^{-1}$, $c_0 = 4\mathrm{MPa}$, the latter representing the values typical for some sedimentary rocks (Hoek and Brown, 1980). The primary objective of the study reported here is to examine the sensitivity of the conditions at failure to the distribution of material parameters, i.e. a and c, equation (2.4), as well as the varying confining pressure p_0.

Figure 2.2 shows the variation of axial strength and the orientation of the localization plane as a function of the orientation of the sample. The simulations correspond to $\Omega^a_{ij} = \Omega^c_{ij} = \Omega_{ij}$, and the degree of anisotropy is defined in terms of $\Omega_1 = \Omega_3$, while $\Omega_1 + \Omega_2 + \Omega_3 = 0$ (traceless condition). It is evident from this figure that the strength is the highest for β=90°. For inclined specimens, the strength reaches a minimum at $\beta \approx 35°$. The orientation of the localization plane ranges between 54° and 59° and is affected by both the degree of anisotropy and the orientation of the sample.

The results shown in figure 2.3 correspond to $a = a_0 =$ const., while those shown in figure 2.4 pertain to $c = c_0 =$ const. Clearly, the distribution of material properties affects both the evolution of axial strength as well as the orientation of the failure plane. Depending on the case, the angle specifying the orientation of the localization plane is either positive or negative, implying that the plane is located in a different quadrant in space. Also, the distribution of axial strength is significantly affected, so that the extreme values correspond to different orientations of the sample.

Figure 2.5 shows the curves corresponding to various confining pressures p_0 . The simulations incorporate a set of material parameters analogous to those provided in figure 2.2. It is evident here that the strength significantly increases with p_0, while the nature of the distribution remains the same as before. Finally, figure 2.6 presents the results for Tresca material, equation (2.8). Here, the distribution of axial strength displays symmetry about β=45°, at which point the minimum strength is reached. At the same time, at β=45° the localization plane is also at 45°, irrespective of the degree of anisotropy. Overall, the qualitative aspects of the behaviour identified here appear to be consistent with the trends reported by Baker and Krizek (1970).

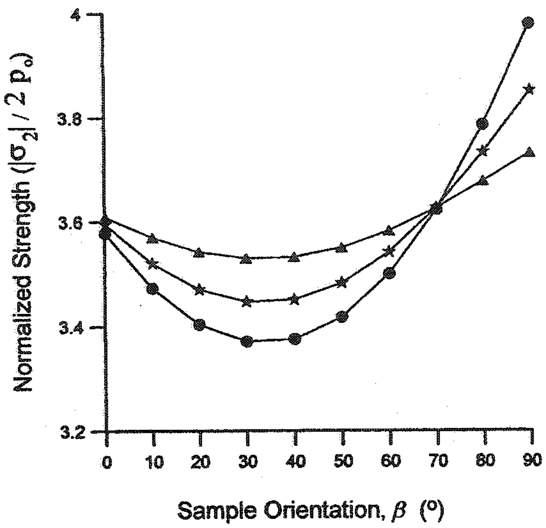

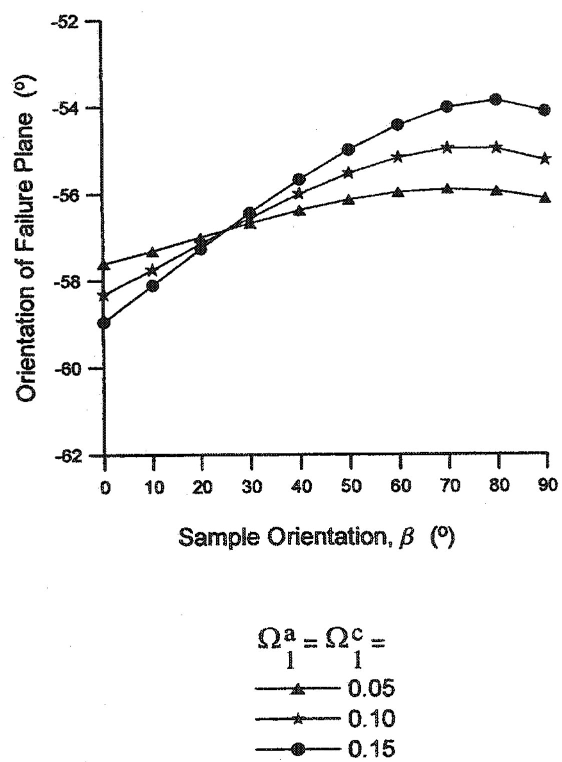

Figure 2.2 Variation of axial strength and orientation of failure plane with sample orientation (critical plane approach; eq. 2.1, $b_o = 0$, $a_o = 0.04\,(MPa)^{-1}$, $c_o = 4\,MPa$, and $p_o = 10\,MPa$).

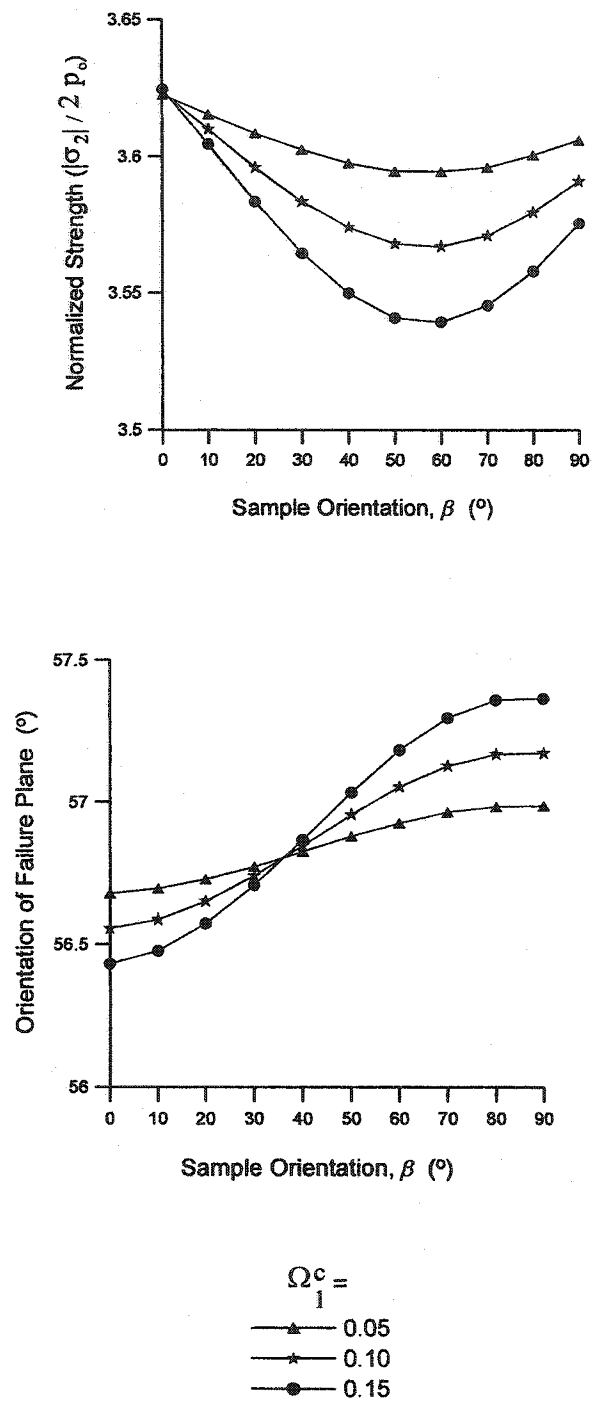

Figure 2.3 Variation of axial strength and orientation of failure plane with sample orientation (critical plane approach; eq. 2.1, $b_0 = 0$, $a = const. = 0.04\ (MPa)^{-1}$, $c_o = 4\ MPa$, and $p_o = 10\ MPa$).

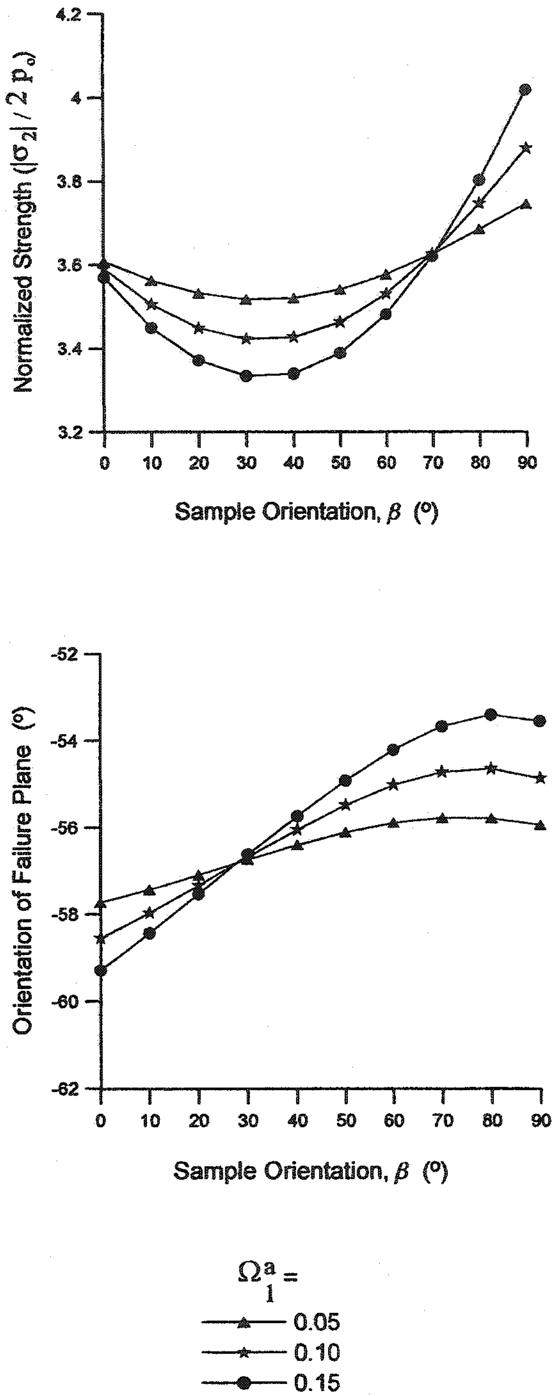

Figure 2.4 Variation of axial strength and orientation of failure plane with sample orientation (critical plane approach; eq. 2.1, $b_o = 0$, $a_o = 0.04\,(MPa)^{-1}$, $c = const. = 4\,MPa$, and $p_o = 10\,MPa$).

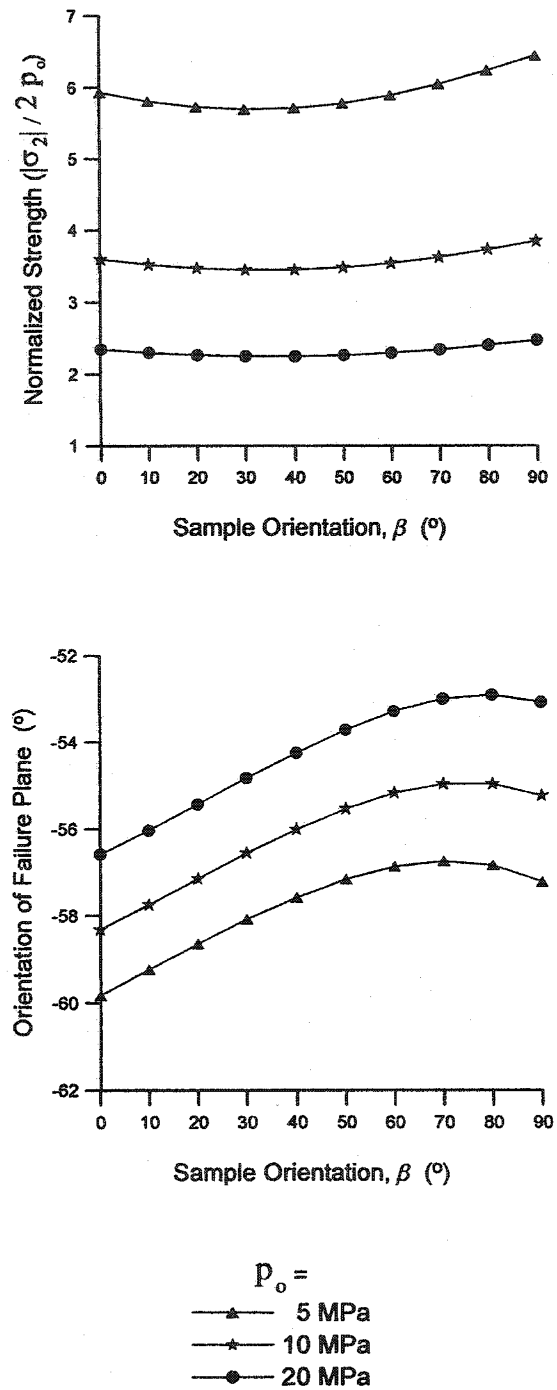

Figure 2.5 Variation of axial strength and orientation of failure plane with sample orientation for different confining pressures (critical plane approach; eq. 2.1, $b_o = 0$, $a_o = 0.04\,(MPa)^{-1}$, $c_o = 4\,MPa$, and $\Omega_1^a = \Omega_1^c = 0.1$).

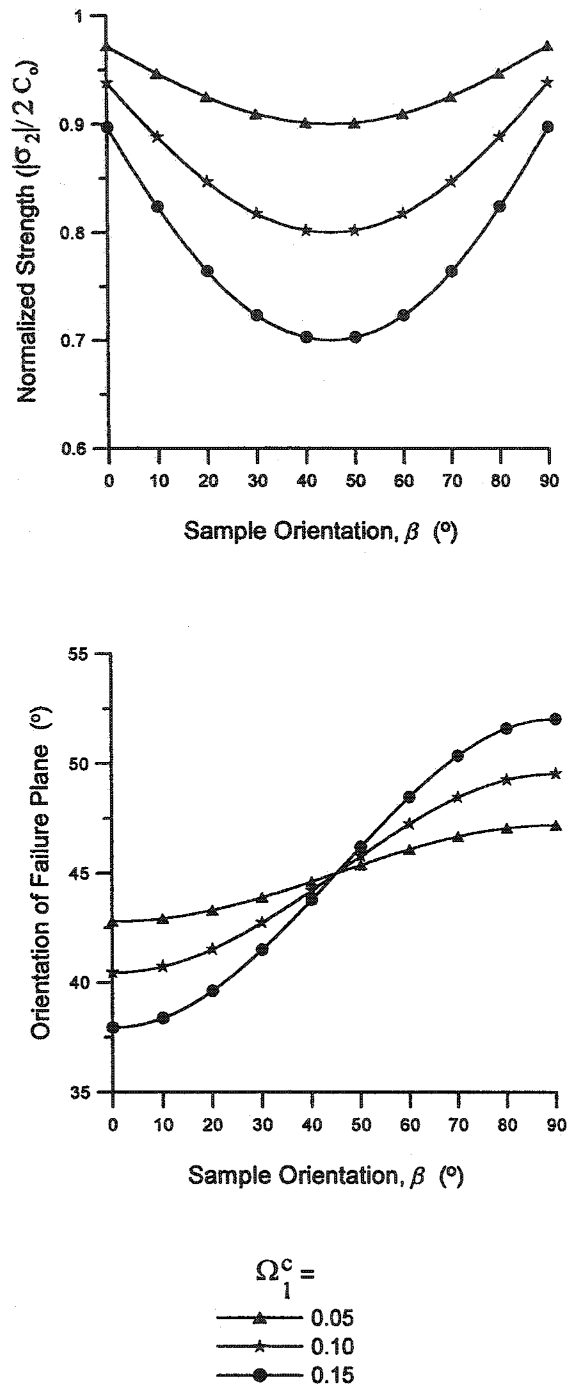

Figure 2.6 Variation of axial strength and orientation of failure plane with sample orientation (critical plane approach; *Tresca* material).

2.2 Formulation of a Macroscopic Failure Criterion for Structural Masonry

A typical element of structural masonry consists of brick units interspersed by two orthogonal sets of *bed* and *head joints* filled with mortar, figure 2.7. Masonry exhibits strong directional properties since the mortar joints act as planes of weakness. Most masonry structures, such as arch bridges, infilled walls in framed constructions, etc., are subjected to low confining pressures. Consequently, the conditions at failure in a representative volume may be described by employing a bi-linear approximation to the quadratic form (2.1). Consider the following failure function in terms of normal and tangential components of the traction vector on a plane with unit normal n_i

$$\text{in tension domain } (\sigma \geq 0), \quad F = |\tau| + \mu^t(\sigma - \sigma_0) = 0$$

$$\text{in compression domain } (\sigma < 0), \quad F = |\tau| + \mu^c\sigma - \mu^t\sigma_0 = 0 \tag{2.11}$$

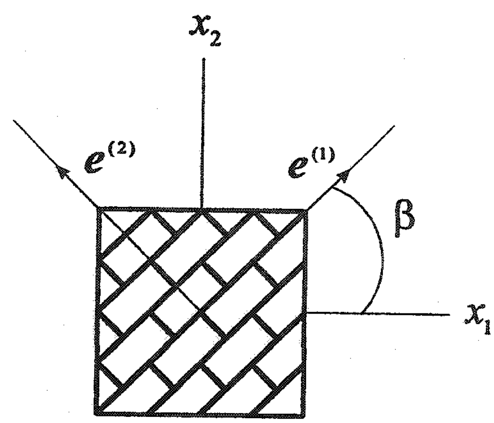

Figure 2.7 Geometry of the problem for structural masonry.

The geometric representation of equation (2.11) is provided in figure 2.8. The parameter μ^c acts as a coefficient of friction in compression domain, μ^t is the slope of the failure envelope in the tension domain, whereas σ_0 represents the tensile strength in the direction normal to the plane.

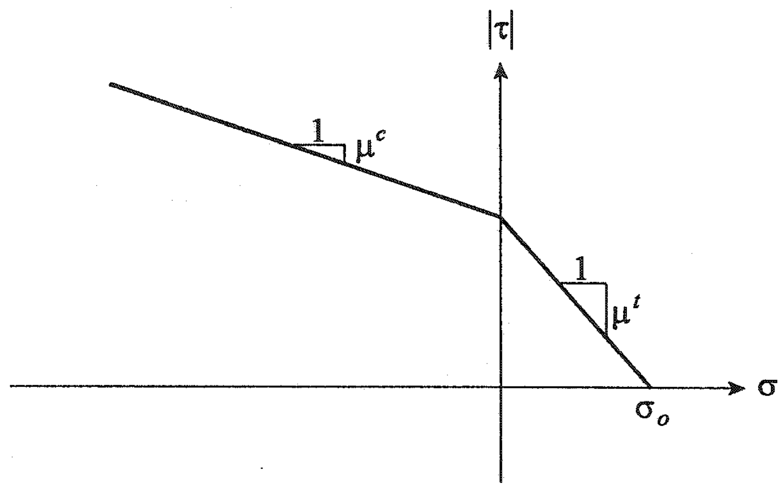

Figure 2.8 Bilinear failure envelope for structural masonry.

Equation (2.11) may be restated as follows

$$F = \tau + \mu\sigma - \mu^t\sigma_0 = 0 \tag{2.12}$$

where

$$\mu = \mu^t \quad \text{for } \sigma \geq 0; \qquad \mu = \mu^c \quad \text{for } \sigma < 0 \tag{2.13}$$

Assume now that the material parameters involved are defined in terms of the distribution functions

$$\mu = \mu_0(1 + \Omega_{ij}^{\mu} n_i n_j), \qquad \mu^t = \mu_0^t(1 + \Omega_{ij}^{\mu^t} n_i n_j)$$

$$\sigma_0 = \sigma_{01}(1 + \Omega_{ij}^{\sigma_0} n_i n_j) + \sigma_{02}(\Omega_{ij}^{\sigma_0} n_i n_j)^2 + \sigma_{03}(\Omega_{ij}^{\sigma_0} n_i n_j)^3 \tag{2.14}$$

Note that the expression for σ_0 incorporates higher order dyadic products of $\Omega_{ij}^{\sigma_0} n_i n_j$. This allows for a more accurate representation of the material behaviour as pointed out by Pietruszczak and Mroz (2001).

Incorporating now the Lagrange multipliers to account for the constraints (2.5), the Lagrangian function is as follows

$$\begin{aligned} G = {} & \sigma_{jk} n_j s_k + \mu_0(1 + \Omega_{jk}^{\mu} n_j n_k)(\sigma_{pq} n_p n_q) - \mu_0^t \sigma_{01}(1 + \Omega_{jk}^{\mu^t} n_j n_k)(1 + \Omega_{pq}^{\sigma_0} n_p n_q) \\ & - \mu_0^t \sigma_{02}(1 + \Omega_{jk}^{\mu^t} n_j n_k)(\Omega_{pq}^{\sigma_0} n_p n_q)^2 - \mu_0^t \sigma_{03}(1 + \Omega_{jk}^{\mu^t} n_j n_k)(\Omega_{pq}^{\sigma_0} n_p n_q)^3 \\ & - \lambda_1(n_j n_j - 1) - \lambda_2(s_j s_j - 1) - \lambda_3 n_j s_j \end{aligned} \tag{2.15}$$

The conditions for a stationary value of this function with respect to n_i and s_i lead to the following set of equations

$$\frac{\partial G}{\partial n_i} = \sigma_{ij}s_j + 2\mu_0(\Omega^{\mu}_{ij}n_j)(\sigma_{pq}n_pn_q) + 2\mu_0(1 + \Omega^{\mu}_{jk}n_jn_k)(\sigma_{iq}n_q) - 2\mu^t_0\sigma_{01}(\Omega^{\mu^t}_{ij}n_j)$$

$$\times(1 + \Omega^{\sigma_0}_{pq}n_pn_q) - 2\mu^t_0\sigma_{01}(1 + \Omega^{\mu^t}_{jk}n_jn_k)(\Omega^{\sigma_0}_{ip}n_p) - 2\mu^t_0\sigma_{02}(\Omega^{\mu^t}_{ij}n_j)(\Omega^{\sigma_0}_{pq}n_pn_q)^2$$

$$- 4\mu^t_0\sigma_{02}(1 + \Omega^{\mu^t}_{jk}n_jn_k)(\Omega^{\sigma_0}_{pq}n_pn_q)(\Omega^{\sigma_0}_{is}n_s) - 2\mu^t_0\sigma_{03}(\Omega^{\mu^t}_{ij}n_j)(\Omega^{\sigma_0}_{pq}n_pn_q)^3$$

$$- 6\mu^t_0\sigma_{03}(1 + \Omega^{\mu^t}_{jk}n_jn_k)(\Omega^{\sigma_0}_{pq}n_pn_q)^2(\Omega^{\sigma_0}_{is}n_s) - 2\lambda_1n_i - \lambda_3s_i = 0$$

$$\frac{\partial G}{\partial s_i} = \sigma_{ij}n_j - 2\lambda_2s_i - \lambda_3n_i = 0 \qquad (2.16)$$

which together with equation (2.5) can be solved to define the orientation of the localization plane along which F is maximum.

2.3 Numerical Analysis

In this section, the results of numerical simulations are presented for the verification of the proposed failure criterion (2.11). First, some comments are provided on the identification of material parameters/functions involved. Subsequently, in section 2.3.2, the numerical results for axial compression and tension at different orientations of the bed joints relative to the loading direction are presented. The predictions corresponding to in-plane biaxial tension-compression and compression-compression are also discussed in this section. The numerical results are compared with the experimental data reported by Page (1981, 1983).

2.3.1 Identification of Material Parameters

The mathematical formulation developed in section 2.2 incorporates a set of material parameters embedded in the distribution functions (2.14). It has to be emphasized that regardless of which set of experimental data is used for the identification purpose, the existing information is inadequate to directly identify all the constants involved. Therefore, some intuitive assumptions need to be incorporated.

The material parameters appearing in equations (2.14) have been selected based on experimental data provided by Page (1983). In general, the experimental results involve in-plane loading conditions only, i.e. biaxial tension-compression, compression-compression, etc. No information is thus provided on the out-of-plane behaviour. Given this restriction, it was assumed that the material is transversely-isotropic. This approximation has little influence on characteristics in biaxial tension-compression, where the failure mode involves formation of an in-plane rupture surface. On the other hand, however, it will affect the predictions in biaxial compression-compression. The latter issue is addressed later in this section, when the analysis is extended for the case of orthotropy.

Given the geometric arrangement of the brick units, it is evident that the principal material triad will coincide with the direction of weakness planes, i.e. the bed and head joints. For a transversely isotropic material, the distribution function describing the variation of axial tensile strength, equation (2.14), incorporates four independent parameters, i.e. σ_{01}, σ_{02}, σ_{03} and $\Omega_1^{\sigma_0}$. Based on the experimental evidence (Page, 1983), it was assumed that the tensile strength in the direction normal to the bed and head joints is 0.24MPa and 0.4MPa, respectively. Furthermore, it is apparent that the tensile strength of the brickwork will significantly increase when the failure plane penetrates through the units. In view of the lack of direct experimental evidence, the remaining two points were chosen in such a way so that the ratio of the tensile strengths on planes inclined at 45° and along the bed joints, respectively, is in the range of 3-4, which according to Page (1983) represents the ratio of brick/mortar axial strengths. The latter assumption resulted in the following set of parameters

$$\sigma_{01} = 0.88\ \text{MPa},\ \ \sigma_{02} = -5.34\ \text{MPa},\ \ \sigma_{03} = 0.60\ \text{MPa},\ \ \Omega_1^{\sigma_0} = -0.226$$

and the corresponding distribution function $\sigma_0(n_i)$ is depicted in figure 2.9a. As shown later in this section, this function ensures that the failure mechanism in axial tension involves the rupture of either bed or head joints, which is confirmed by the experimental evidence.

The identification of the remaining material parameters, equation (2.14), requires in general a set of direct shear tests performed along different orientations. Given the fact that no such tests are available, an implicit approach has been adopted whereby the range of values of the parameters involved was estimated based on the data reported by Page (1983). Subsequently, these values have been adjusted, by trial and error, to fit the actual distribution of axial tensile and compressive strengths. The results of tensile tests provided by Page indicate that for sample orientations of 45° and 67.5°, the failure takes place along the bed joints. From these results the average value of μ^t was estimated to be in the range of 2, whereas the value corresponding to failure along the head joints was assessed to be about 20% higher. Furthermore, in order to simplify the problem, it was assumed that $\mu^c = \mu_c^0 = \text{const}$. Given the information on samples tested at 45° and 67.5° in compression regime, which involved failure along the bed joints, μ_c^0 was estimated to be in the range of 1. Starting with the above estimates, the final values adopted through the trial and error procedure were as follows

$$\mu_0^t = 2.4, \quad \Omega_1^{\mu^t} = 0.06, \quad \mu_0^c = 1.1$$

The corresponding distribution of μ^t is given in figure 2.9b.

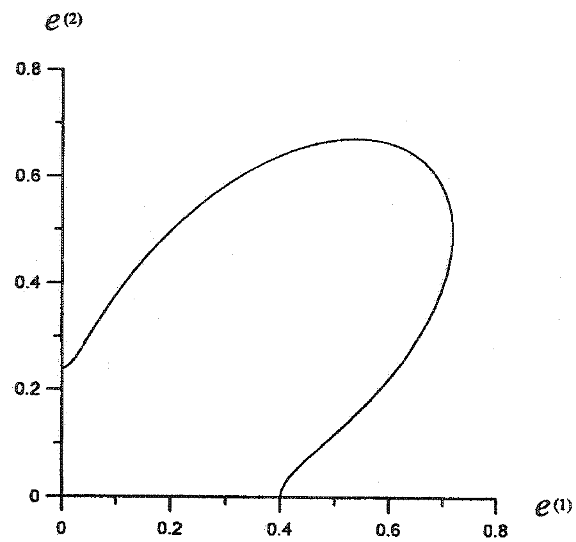

(a)

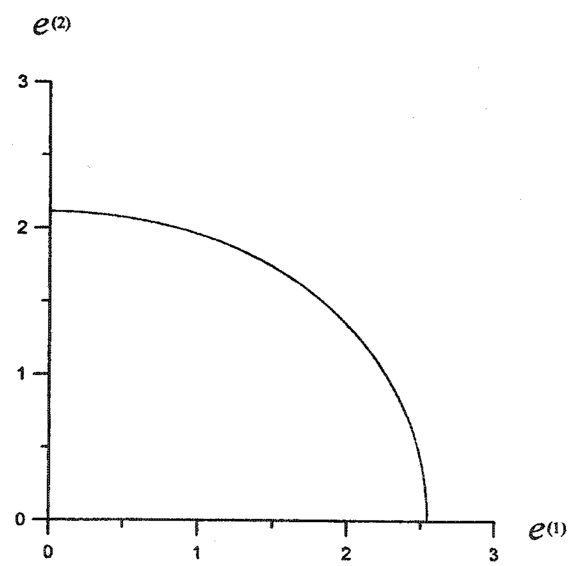

(b)

Figure 2.9 Polar distributions for (a) σ_o (values in MPa), and (b) μ'.

2.3.2 Numerical Results

The values of the material parameters specified in the preceding section have been incorporated to carry out extensive numerical simulations in both compression and tension regimes. First, the behaviour under axial tension has been examined. Figure 2.10a shows the variation of tensile strength as a function of the orientation of bed joints. At the same time, figure 2.10b depicts the change in the orientation of the failure plane. It is evident from this figure that for low values of β (within the range from 0° to 30°) the failure of the brickwork is induced by the rupture of the head joints. In this case, the tensile strength does not change significantly, figure 2.10a. For β exceeding 40°, the failure occurs in the bed joints and the tensile strength of the brickwork drops significantly. The results are consistent with the experimental data provided by Page, particularly in the context of the transition in failure mode. It should be noted that the experimental data shows a significant scatter. In general, however, the range of values of the tensile strength and the trend in the distribution is similar to that predicted by the linear form (2.11).

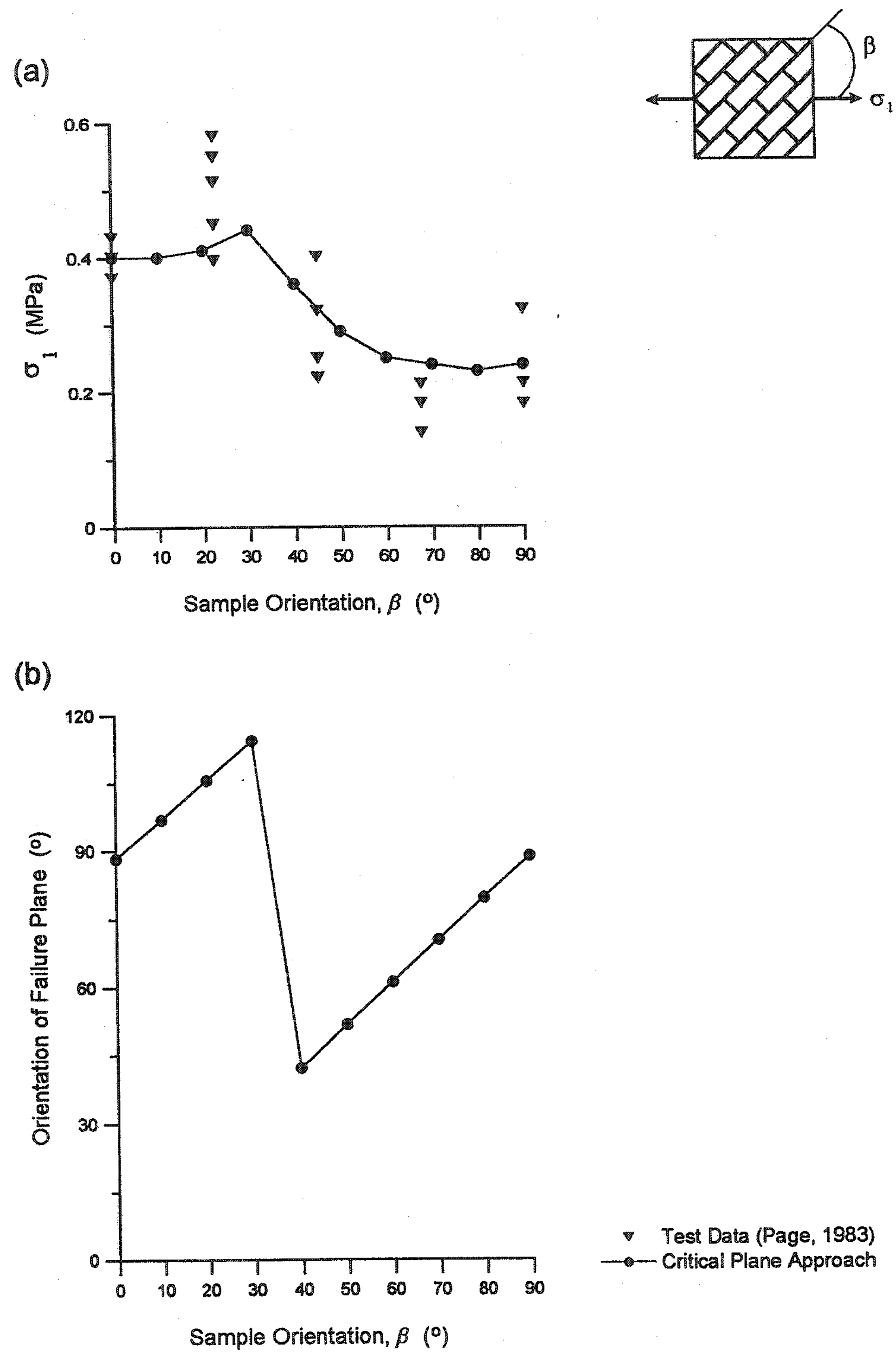

Figure 2.10 Variation of uniaxial tensile strength and orientation of failure plane with sample orientation.

The next stage involves the simulations of axial compression tests performed at different orientation of the bed joints, figure 2.11. The results shown in figure 2.11b indicate that for low values of β, the failure occurs through formation of a macrocrack in the bricks in the direction which is in a close proximity to the head joints. In this range, the compressive strength first decreases, reaching a minimum at $\beta \approx 22.5°$, and then progressively increases, figure 2.11a. The minimum strength is actually associated with the localization plane which is in the direction of head joints. At $\beta \approx 40°$, a transition in the failure mode takes place, whereby the failure plane is shifted to the region in the vicinity of the bed joints. In this case, a similar trend is observed, i.e. the compressive strength is initially reduced, reaching a minimum at $\beta \approx 67.5°$, which is associated with localization of failure in the bed joints. For higher values of β, the failure mode involves, once again, formation of a macrocrack penetrating through the bricks, and the resulting compressive strength increases. The predicted behaviour is, in general, in a good agreement with the data of Page (1983). The trends are also consistent with the results of experimental tests reported by Drysdale and Khattab (1995).

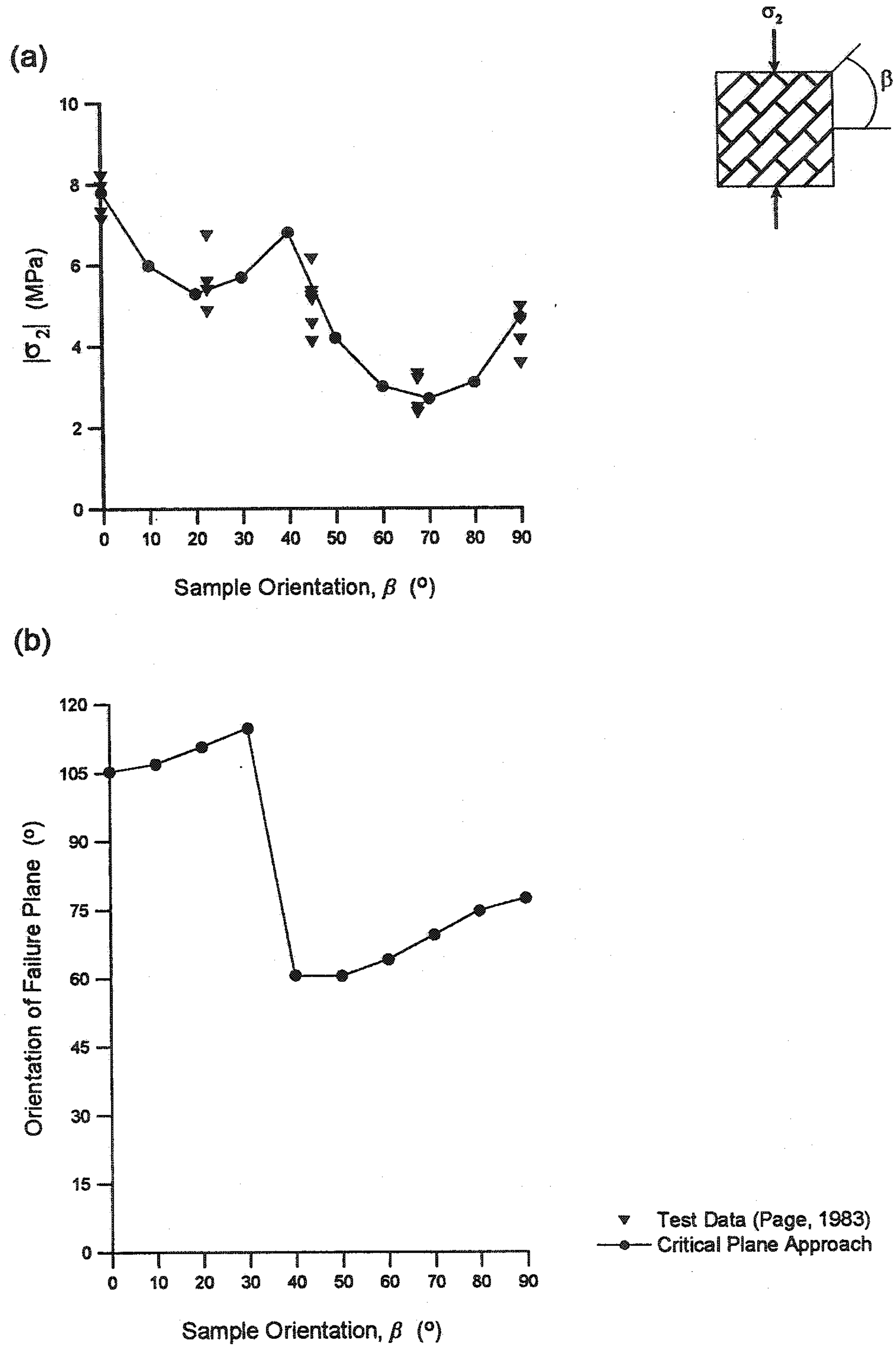

Figure 2.11 Variation of uniaxial compressive strength and orientation of failure plane with sample orientation.

The subsequent set of simulations involves the predictions of a series of in-plane biaxial compression-tension tests as conducted by Page (1983). The loading process involves a number of trajectories corresponding to a constant ratio of compressive to tensile stress. Again, the simulations have been performed for different orientations of the sample relative to the loading direction. The results are reported in figure 2.12, which shows the predicted failure envelopes. It is evident that the trends are again fairly consistent with the experimental data.

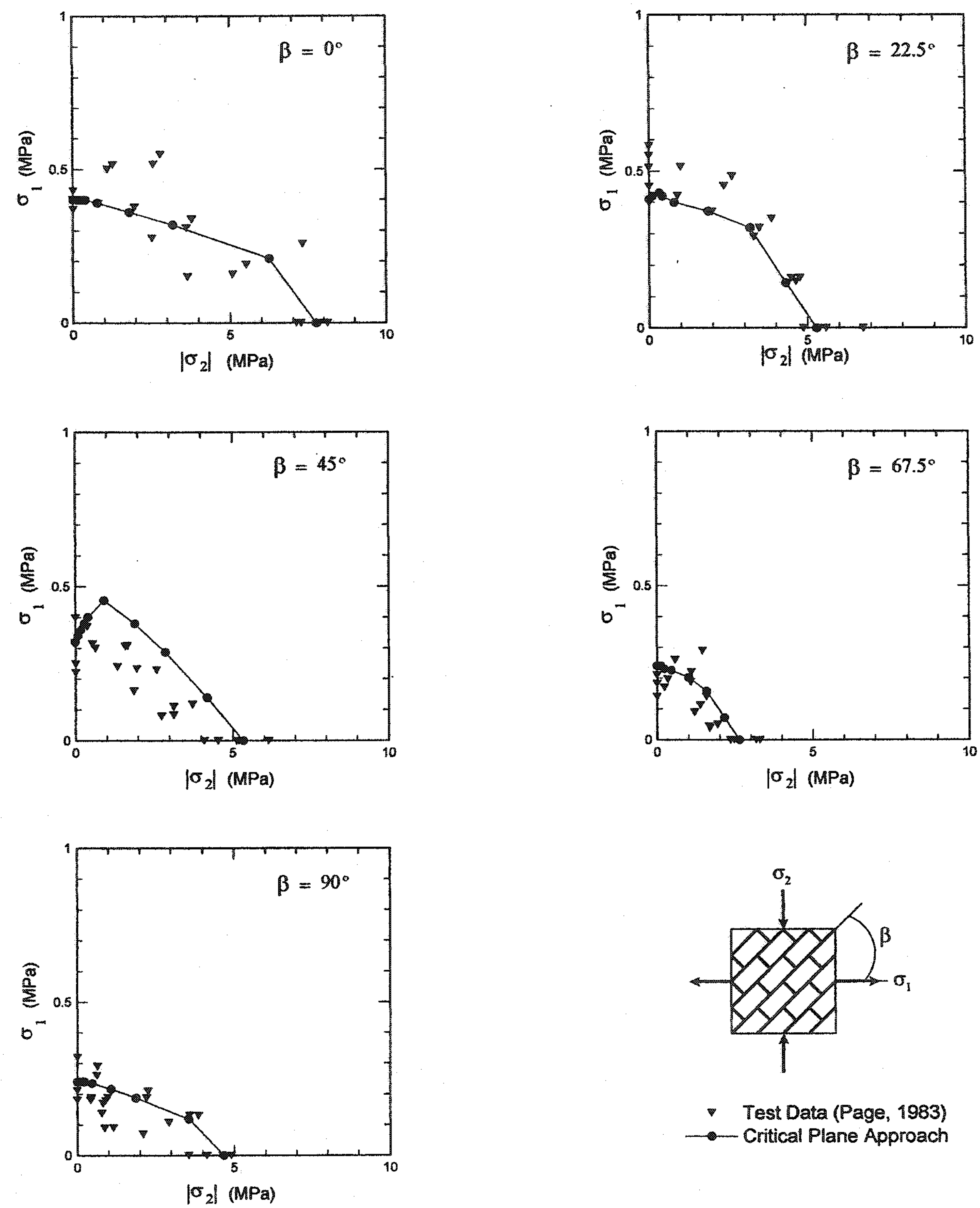

Figure 2.12 Failure envelopes for in-plane biaxial compression-tension tests.

Finally, figure 2.13 shows a set of predictions corresponding to biaxial compression programs. The experimental results are taken from an earlier work of Page (1981). It should be noted that for the loading histories employed here, the out of plane stress, which is equal to zero, is actually the minor principal stress. Consequently, the failure mode in this series of tests is typically associated with formation of an out-of-plane rupture surface and subsequent splitting of the sample. In this context, the assumption of transverse isotropy, as employed in the identification procedure, has a profound effect on the numerical predictions. It is apparent from figure 2.13 that, for a broad range of stress ratios, irrespective of the orientation of the sample, the strength is significantly underestimated. In view of this, an additional set of simulations have been carried out, assuming that the distribution of μ^t exhibits orthotropic properties. In particular, the analysis has been performed assuming that the out-of-plane value of μ^t is higher than that stipulated by the transversely-isotropic distribution, i.e. $\mu^t(x_3)=3.3$, while the in-plane characteristics (figure 2.9b) are not altered. This corresponds to the following set of parameters

$$\mu_0^t = 2.65, \quad \Omega_1^{\mu^t} = -0.041, \quad \Omega_2^{\mu^t} = -0.204$$

It is evident from figure 2.13 that the resulting failure envelope, shown by a broken line, is in a better agreement with the experimental tests. Thus, it is apparent that for predicting the behaviour of structural masonry under in-plane biaxial compression-compression, the out-of-plane characteristics of the sample play an important role and should be considered in identification of the relevant material parameters.

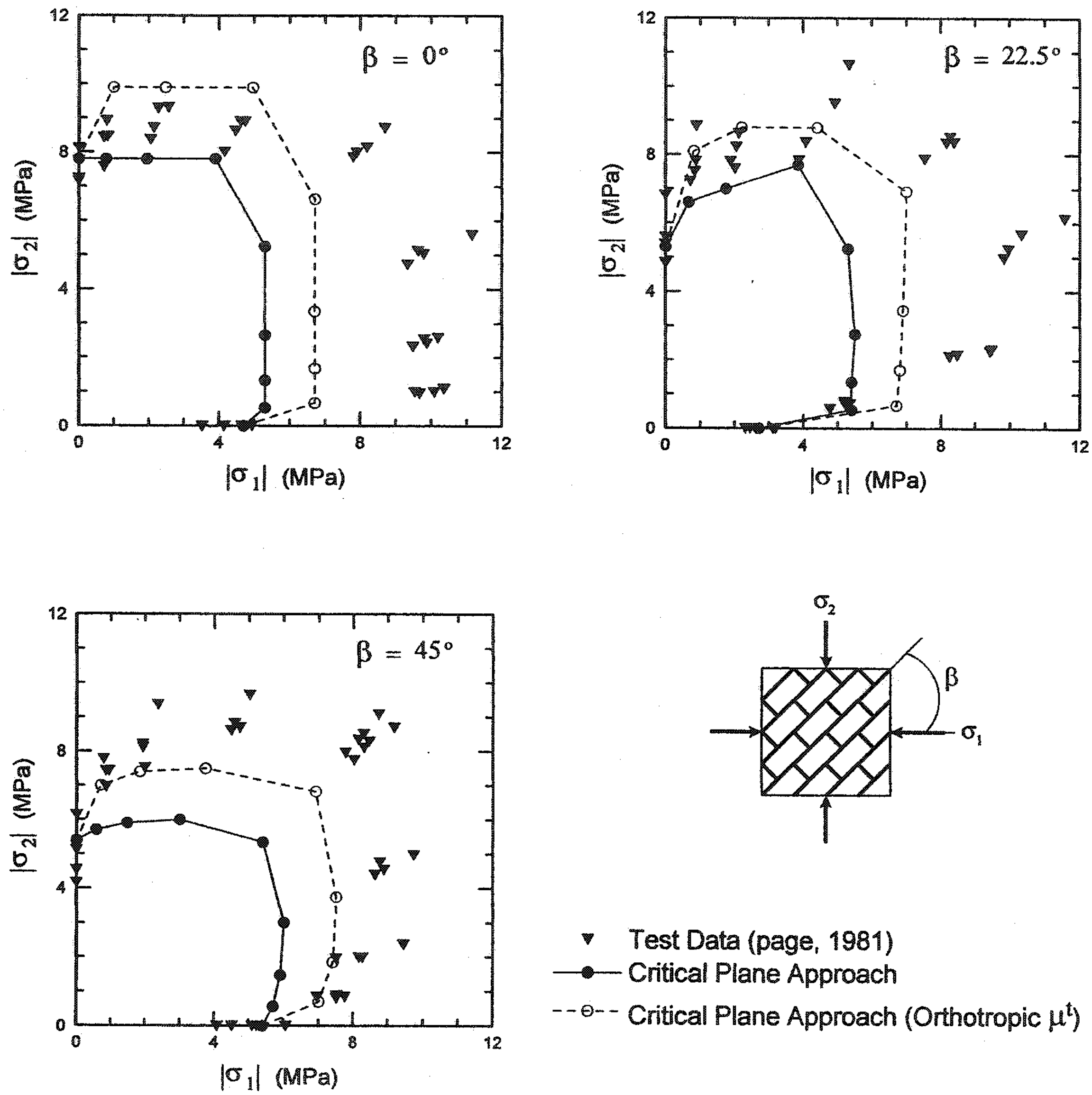

Figure 2.13 Failure envelopes for in-plane biaxial compression tests.

CHAPTER 3

SEISMIC ANALYSIS OF BRICK MASONRY WALLS OF A POWER SUBSTATION BUILDING

In this chapter, the macroscopic failure criterion for structural masonry discussed in chapter 2 is incorporated in a 3D seismic analysis of masonry walls of a power substation building (Gocevski et al., 2002). The power substation is similar, in terms of geometry and the structural arrangement, to the Saraguay substation, located in the north-western part of the Montreal Island in Quebec, Canada. Its principal function is to step the transmission voltages from Hydro-Quebec's transportation network down to the distribution voltage and split the distribution power off in multiple directions. The substation is of a strategic importance since it supplies the electricity for six secondary substations serving 480,000 clients. The main building, which houses the command panels for the substation, was constructed in 1957. It is a one-floor structure with the dimensions 32m × 27m. The exterior bearing walls, with the height of 5.11m, are made of unreinforced masonry.

The main purpose here is to examine the performance of masonry walls of the power substation described above, under the conditions of seismic excitation. The analysis presented here is conducted in the elastic range assuming orthotropic material properties. These have been estimated based on a homogenization procedure outlined in the article by Pietruszczak & Niu (1992). The plastic admissibility of the resulting stress field is assessed by incorporating the macroscopic failure criterion outlined in the previous chapter. In what follows, the numerical results are presented, including the examination of various reinforcement strategies.

The dynamic analysis is conducted for the ground motion history depicted in figure 3.1, which is representative of 1988 Saguenay earthquake.

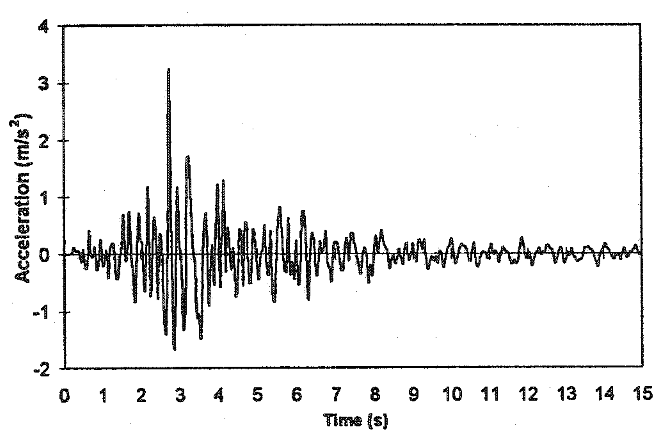

Figure 3.1 History of base acceleration.

Figure 3.2 shows the finite element discretization of the structure. The finite element mesh incorporates a combination of 8-noded solid elements (masonry walls and concrete base), 3D beam elements (the roof truss) and 3D shell elements (the roof cover and the concrete beam above the window openings). The total of about 9,300 elements are used. The loading consists of two main stages. First, the initial stresses due to self weight of the structure are determined. Subsequently, a dynamic analysis is conducted simulating the seismic event. For the latter stage, the maximum horizontal acceleration, in the direction along the diagonal of x,z-plane, is fixed at 0.193g, whereas the maximum vertical component is taken as 0.03g.

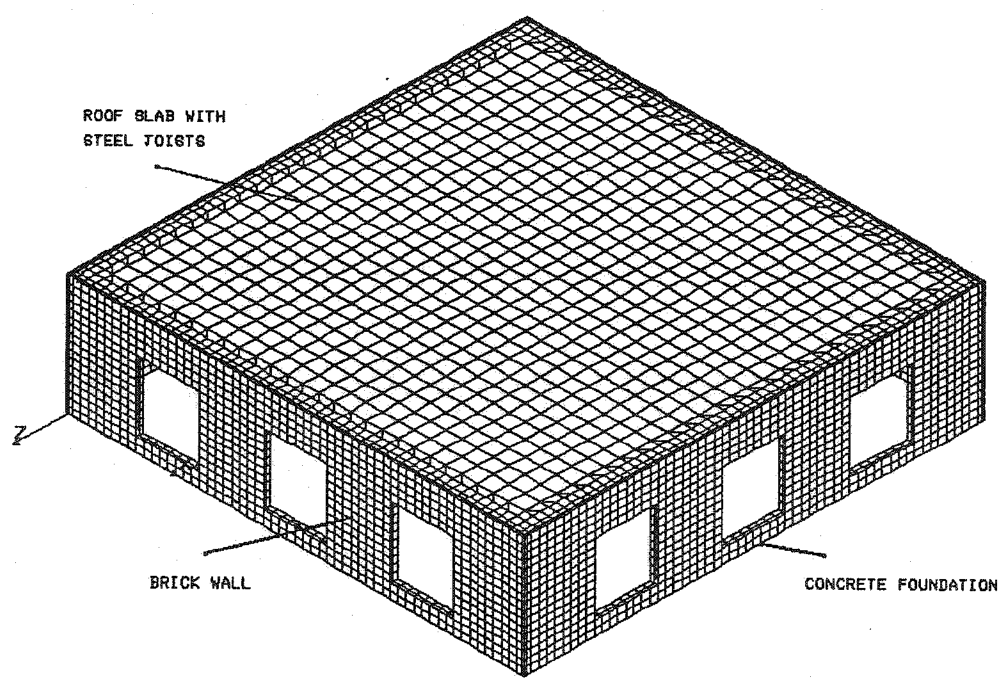

Figure 3.2 Finite element discretization of the structure.

Figure 3.3 shows the distorted mesh together with the superimposed distribution of horizontal displacements at the time interval corresponding to the maximum base acceleration. In general, the focus of the analysis here is on the load bearing walls, which run in the direction along the x-axis. It is evident from the figure that the earthquake produces a significant distortion of the brickwork. The most affected are the regions in the centre of the wall, above the window openings.

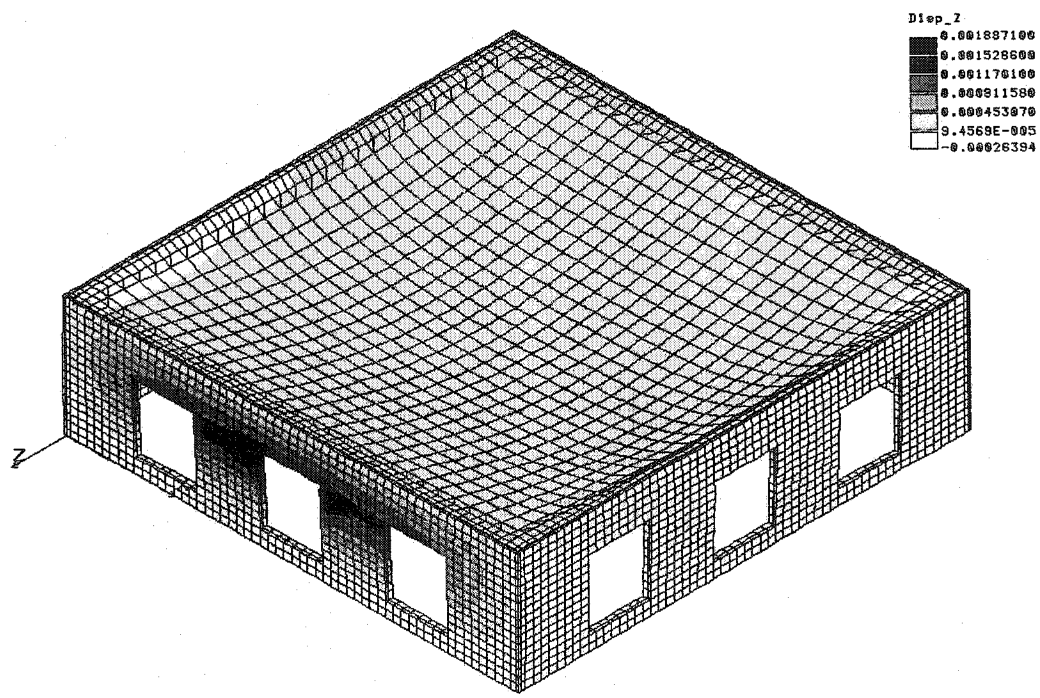

Figure 3.3 Distorted mesh; distribution of the horizontal displacement in the bearing wall.

Figure 3.4a shows the maps of the value of the failure function, equation (2.1), along the face of the bearing wall. The nature of the distribution is consistent with the deformation mode depicted in figure 3.3. The regions above and adjacent to the openings experience $F>0$, which indicates that the stress field is plastically inadmissible, i.e. may result in the failure of the brickwork. The regions of tension/compression, as identified based on the failure criterion, are sketched in Figure 3.4b. Comparing the two distributions, it is evident that the states of $F>0$ are associated predominantly with the tension regime.

(a)

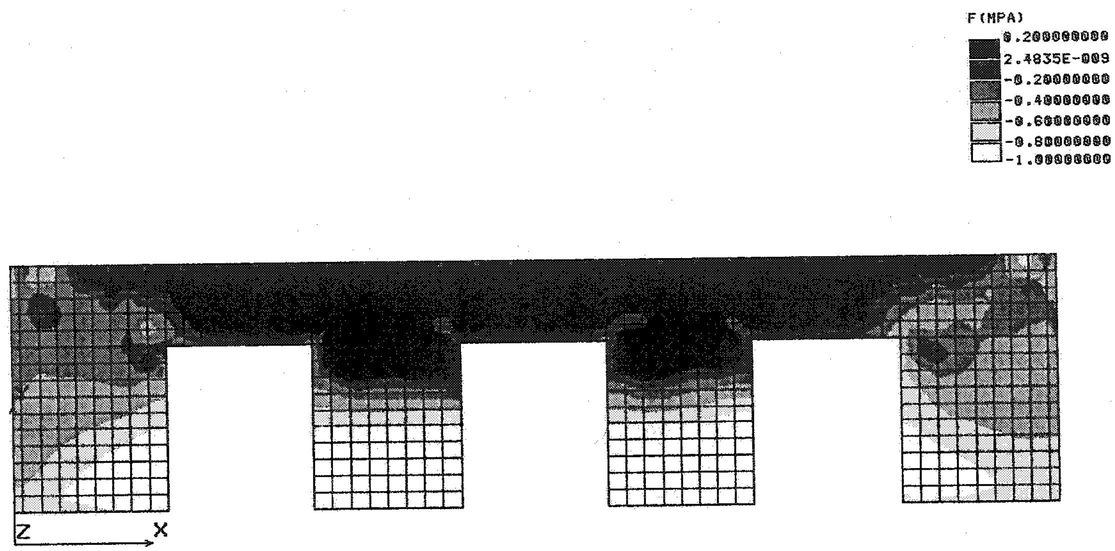

(b)

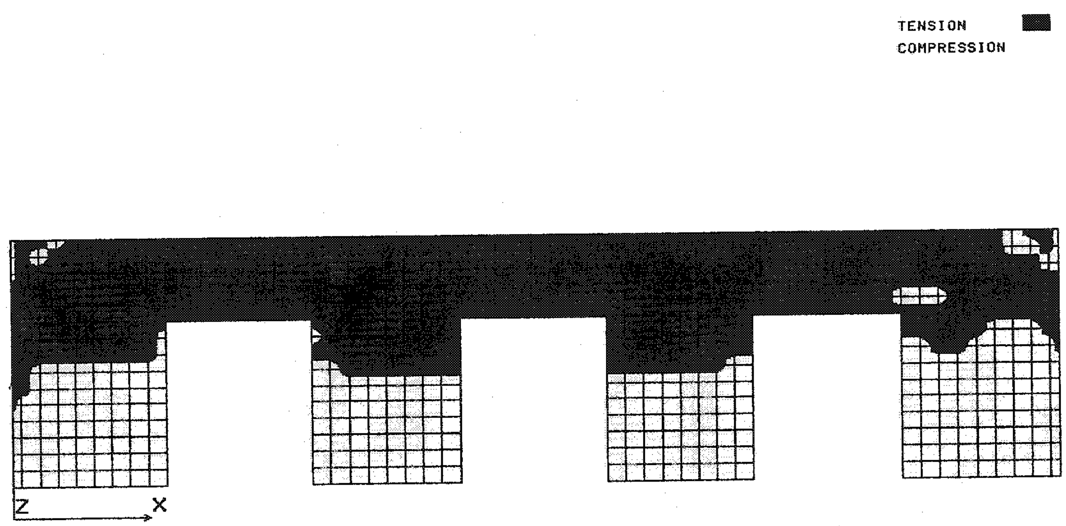

Figure 3.4 Distribution of (a) failure function, and (b) tension/compression domains.

In order to improve the stability of the wall, two separate reinforcement scenarios have been considered. The first one involved the placement of steel bracings behind the critical sections of the brickwork, as indicated in figure 3.5a. The horizontal/vertical braces and the cross-braces incorporated W360×122 and L152×89×9.5 sections, respectively, and are discretized using 3D beam elements. The steel columns, once in place, are assumed to be jacked-up in order to ensure that the load exerted by the roof structure is transferred directly to the added steel bracing system. The resulting distribution of the failure function is shown in Figure 3.5b. Clearly, this reinforcement strategy is quite effective, owing to the fact that the overall stability does no longer rely on the resistance of the bearing walls alone.

The second reinforcement scenario involved a placement of 0.06m thick shotcrete concrete walls, which were attached to the brickwork by steel plates (pl 30mm × 2mm × 60 mm long) spaced at 600 mm c/c, figure 3.6a. This is a frequently used method for assuring the integrity of non-reinforced masonry walls. The shotcrete walls are modelled using 8-noded solid elements. Figure 3.6b shows the resulting distribution of the failure function. The regions adjacent to the openings still experience $F>0$, which indicates that the stress field is plastically inadmissible, i.e. may result in a local failure of the brickwork. Since in this case the bearing walls are the sole support for the roof, the stability of the building cannot be strictly ensured.

(a)

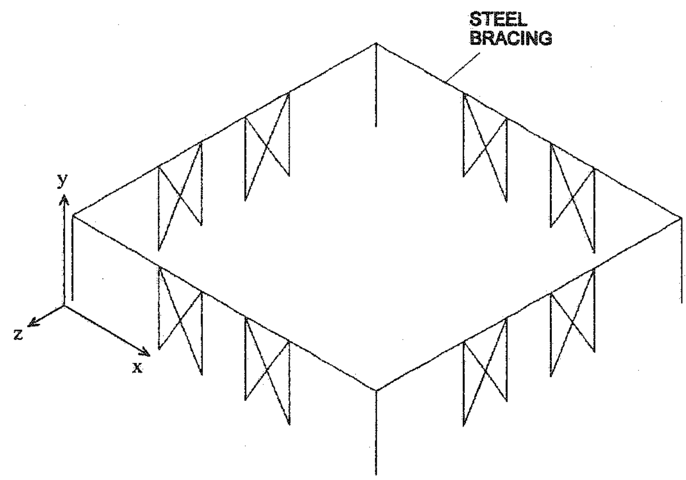

(b)

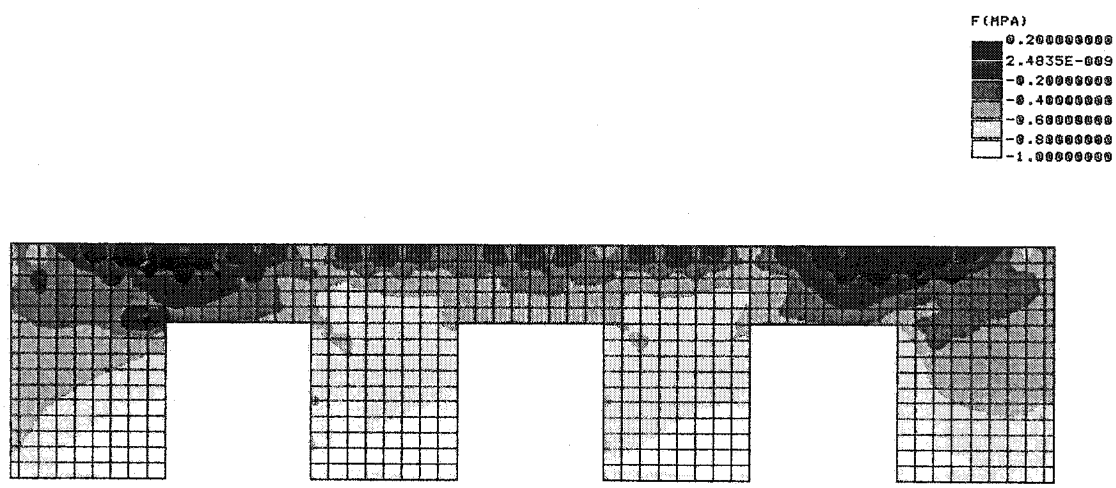

Figure 3.5 Distribution of failure function (wall reinforced with steel bracings).

(a)

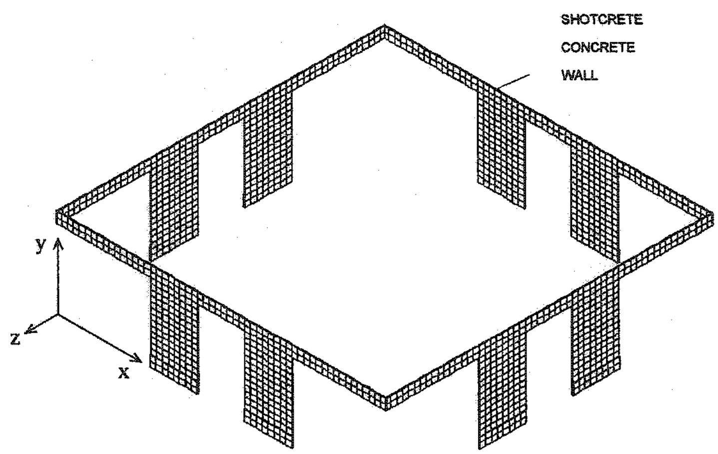

(b)

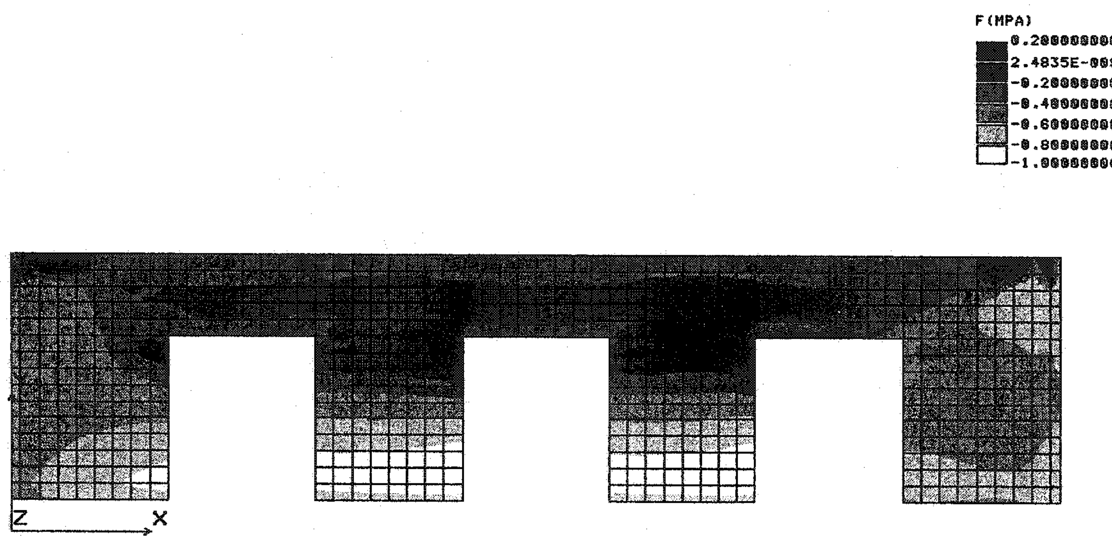

Figure 3.6 Distribution of failure function (reinforced with shotcrete concrete walls).

CHAPTER 4

DESCRIPTION OF INELASTIC BEHAVIOUR OF STRUCTURAL MASONRY

The main objective of this chapter is to develop a continuum theory for describing the inelastic behaviour of structural masonry. The approach presented here (Pietruszczak and Ushaksaraei, 2002) may be perceived as a pragmatic alternative to the homogenization method. It is simpler in numerical implementation and addresses all stages of the deformation process, including the localized deformation associated with formation of macrocracks. In section 4.1, a general formulation of the problem is provided. The conditions at failure are described by invoking a critical plane approach, as discussed in chapter 2. This approach is subsequently extended to incorporate the inelastic deformation (section 4.1.2). This is accomplished by attributing the inelastic response to sliding/separation along an infinite number of randomly oriented planes. The behaviour along each plane is defined in terms of a plasticity framework and the global macroscopic response is obtained by averaging the contributions from all active planes.

Section 4.1.3 is devoted to the description of localized deformation. The formation of macrocracks is perceived as a localization problem and the formulation is derived by incorporating a homogenization procedure which employs a 'characteristic dimension'. The general mathematical framework is illustrated by some numerical examples provided in section 4.2. Here, the details pertaining to the specification of material functions/parameters are discussed first, followed by numerical analyses examining the response of brickwork in compression and tension regimes for different orientations of the bed joints. Finally, in section 4.3 the results of a finite element analysis of a bearing masonry wall subjected to in-plane loading are presented. Here, the evolution of the crack pattern is examined prior to the collapse of the wall.

4.1 General Formulation

In this section, a mathematical model describing the inelastic response of structural masonry is outlined. Referring again to figure 2.7, a representative volume of the material consists of a large number of masonry units interspersed by two orthogonal families of bed and head joints filled with mortar. The geometry of the problem is described in the global frame of reference $\boldsymbol{x}$, while the principal material triad is defined by the base vectors $\boldsymbol{e}^{(1)}, \boldsymbol{e}^{(2)}, \boldsymbol{e}^{(3)}$.

The general formulation of the problem comprises three main aspects. The first one is related to specification of the conditions at failure, which is accomplished by incorporating a critical plane approach. The second step involves an extension of this approach to model the inelastic deformation. This is achieved by incorporating a multi-laminate framework, in which the response is described in terms of sliding/separation along a set of randomly distributed planes. The last issue involves the description of localized deformation associated with formation of macrocracks.

4.1.1 Failure Locus for Structural Masonry

The conditions at failure are defined by postulating a path-independent criterion introduced in section 2.2. According to this criterion, the failure function, along an arbitrary plane with unit normal n_i, is defined as

$$F = \tau + \mu\sigma - \mu^t \sigma_o = 0;$$
$$\mu = \mu^t \quad for \quad \sigma \geq 0; \qquad \mu = \mu^c \quad for \quad \sigma < 0 \tag{4.1}$$

where the material functions involved are specified in equation (2.14).

The orientation of the localization plane can be determined by maximizing the failure function F, with respect to n_i and s_i, subject to constraints $n_i n_i = 1$, $s_i s_i = 1$, $n_i s_i = 0$. The corresponding Lagrangian function is

$$\begin{aligned}
G = {} & \sigma_{jk} n_j s_k + \mu_o (1 + \Omega^{\mu}_{jk} n_j n_k)(\sigma_{pq} n_p n_q) - \mu^t_o \sigma_{01} (1 + \Omega^{\mu^t}_{jk} n_j n_k)(1 + \Omega^{\sigma_0}_{pq} n_p n_q) \\
& - \mu^t_o \sigma_{02} (1 + \Omega^{\mu^t}_{jk} n_j n_k)(\Omega^{\sigma_0}_{pq} n_p n_q)^2 - \mu^t_o \sigma_{03} (1 + \Omega^{\mu^t}_{jk} n_j n_k)(\Omega^{\sigma_0}_{pq} n_p n_q)^3 \\
& - \lambda_1 (n_j n_j - 1) - \lambda_2 (s_j s_j - 1) - \lambda_3 n_j s_j
\end{aligned} \tag{4.2}$$

The stationary conditions with respect to n_i and s_i, together with the constraints of the problem, provide a set of algebraic equations which can be solved for n_i, s_i, and λ's.

4.1.2 Description of Inelastic Deformation

In this section, the methodology outlined above is extended to incorporate the description of the deformation process. This is accomplished by attributing the inelastic behaviour to sliding/separation along an infinite set of randomly oriented planes. For each plane, the conditions at failure are represented by the local criterion, which incorporates the distribution functions (2.14). The inelastic deformation is then accounted for by invoking an appropriate plasticity formulation. This approach is conceptually similar to the so-called multi-laminate framework (Pande & Sharma, 1983; Pietruszczak & Pande, 1987).

Assume that the yield and plastic potential functions for the *i*-th plane, with unit normal n_i, have a general form

$$f(n_i)=f(\sigma,\tau,\kappa)=0; \qquad \psi(n_i)=\psi(\sigma,\tau)=const. \tag{4.3}$$

where, κ is a hardening parameter, which is a function of the plastic deformation history. The equation of the yield surface is formulated in such a way that $\kappa \to \infty \Rightarrow f \to F \to 0$, so that the conditions at failure are consistent with the representation (4.1).

Introducing a local frame $\bar{x}$ associated with the base vectors n_i and s_i, the flow rule may be written as

$$\dot{\bar{e}}_i^p = \dot{\lambda}\frac{\partial \psi}{\partial \bar{t}_i} \tag{4.4}$$

where $\bar{e}_i$ is the strain vector, whereas the corresponding traction $\bar{t}_i$ has the components $\bar{t}_i=\{\tau,\sigma,0\}$. The strain rates contributed by this plane are expressed as a symmetric part of a dyadic product

$$\dot{\varepsilon}_{ij}^p=\frac{1}{2}(\dot{e}_i^p n_j+\dot{e}_j^p n_i); \qquad \dot{e}_i^p=T_{ij}\dot{\bar{e}}_j^p \tag{4.5}$$

where T_{ij} is the transformation matrix. Thus, substituting (4.4) into (4.5)

$$\dot{\varepsilon}_{ij}^{p} = \frac{1}{2}\dot{\lambda}(T_{ip} n_j + T_{jp} n_i)\frac{\partial \psi}{\partial \bar{t}_p} \tag{4.6}$$

The global macroscopic deformation is obtained by averaging the contributions from all active planes. Thus,

$$\dot{\underset{\sim}{\varepsilon}}_{ij}^{p} = \frac{1}{8\pi}\int_S \dot{\lambda}(T_{ip} n_j + T_{jp} n_i)\frac{\partial \psi}{\partial \bar{t}_p} dS \tag{4.7}$$

In practical implementations, the integration process is carried out numerically by adopting a set of 'sampling planes'. Details concerning the orientation of these planes and the distribution of weight coefficients are provided by Pande & Sharma (1983).

The global constitutive relation may now be obtained by invoking the additivity of elastic and plastic deformation, i.e.

$$\dot{\varepsilon}_{ij} = C_{ijkl}\,\dot{\sigma}_{kl} + \dot{\underset{\sim}{\varepsilon}}_{ij}^{p} \tag{4.8}$$

where C_{ijkl} is the elastic compliance operator. It is noted that this operator may be estimated by invoking a homogenization technique. Several such approaches have been reported in the literature (e.g., Anthoine, 1995; Pietruszczak & Niu, 1992; Pande et al., 1989).

4.1.3 Description of localized deformation

The constitutive relation (4.8) governs the response of the material prior to the onset of a localized deformation mode, which is associated with formation of macrocracks. Within the framework employed here, the localization takes place on a plane for which F=max F and the direction of the macrocrack is identified with that of the critical plane. The behaviour after the inception of localization is described by incorporating an averaging procedure, similar to that developed in Pietruszczak (1999).

Referring to Figure 4.1, consider a representative volume of the material, which comprises now the 'intact' masonry intercepted by a macrocrack of a given orientation n_i.

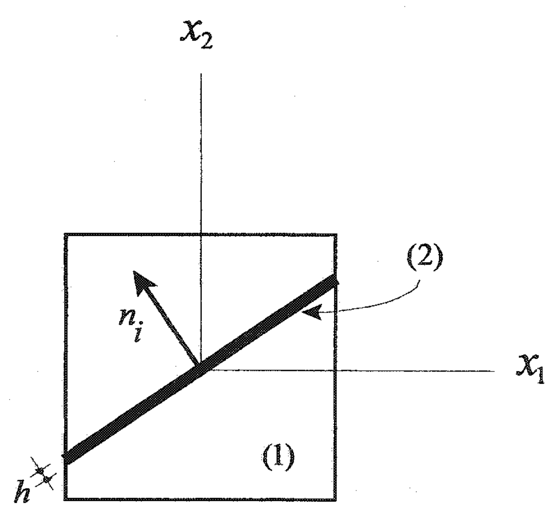

Figure 4.1 Sample intercepted by a macrocrack of orientation n_i.

The formulation of the problem incorporates the stress/strain rate decomposition based on volume averaging

$$\dot{\sigma}_{ij} = \upsilon^{(1)}\dot{\sigma}_{ij}^{(1)} + \upsilon^{(2)}\dot{\sigma}_{ij}^{(2)}; \qquad \dot{\varepsilon}_{ij} = \upsilon^{(1)}\dot{\varepsilon}_{ij}^{(1)} + \upsilon^{(2)}\dot{\varepsilon}_{ij}^{(2)} \tag{4.9}$$

Here, the index (1) refers to the intact material outside the localization zone, (2) denotes the material in the fractured zone and υ's represent the corresponding volume fractions. All quantities are referred to the global coordinate system. The strain rate in the fractured zone may be conveniently defined in terms of velocity discontinuities $\dot{g}_i$, as a symmetric part of a dyadic product

$$\dot{\varepsilon}_{ij}^{(2)} = \frac{1}{2h}(\dot{g}_i n_j + \dot{g}_j n_i) \tag{4.10}$$

where h is the thickness of the macrocrack.

The equilibrium requires that the traction t_i along the discontinuity plane remains continuous. Thus,

$$\dot{t}_i = \dot{\sigma}_{ij}^{(1)} n_j \tag{4.11}$$

Assume now the constitutive relations for both constituents take the general form

$$\dot{\varepsilon}_{ij}^{(1)} = C_{ijkl}\, \dot{\sigma}_{ij}^{(1)}; \qquad \dot{g}_i = K_{ij}\, \dot{t}_j \tag{4.12}$$

It should be noted that since the material in the fractured zone undergoes strain-softening, C_{ijkl} is, in general, an elastic operator as defined by equation (4.8). Substituting now the second relation in equation (4.12) into equation (4.10), and taking into account equation (4.11) gives

$$\dot{\varepsilon}_{ij}^{(2)} = \frac{1}{2h}(K_{ip}n_j n_k + K_{jp}n_i n_k)\dot{\sigma}_{pk}^{(1)} \tag{4.13}$$

Thus, in view of the strain decomposition (4.9)

$$\dot{\varepsilon}_{ij} = \upsilon^{(1)} C_{ijkl}\, \dot{\sigma}_{kl}^{(1)} + \frac{1}{2}\upsilon(K_{ip}n_j n_k + K_{jp}n_i n_k)\dot{\sigma}_{pk}^{(1)} \tag{4.14}$$

where $\upsilon = \upsilon^{(2)}/h$ represents the ratio of the area of the fractured zone to the volume of the sample. Thus the parameter υ is, in fact, independent of h. Noting now that $\upsilon^{(2)} \ll \upsilon^{(1)}$, the stress decomposition in equation (4.9) simplifies to $\dot{\sigma}_{ij} \approx \upsilon^{(1)}\dot{\sigma}_{ij}^{(1)} \approx \dot{\sigma}_{ij}^{(1)}$. Therefore, equation (4.14) can be approximated by

$$\dot{\varepsilon}_{ij} = [C_{ijpk} + \frac{1}{2}\upsilon(K_{ip}n_j n_k + K_{jp}n_i n_k)]\dot{\sigma}_{pk} \tag{4.15}$$

which provides the required macroscopic constitutive relation.

4.2 Numerical Simulations

In this section, the constitutive relations formulated above have been implemented in a numerical code in order to investigate the response of structural masonry panels in a series of axial compression/tension tests. The simulations have been carried out for different orientations of the bed joints relative to the loading direction. Whenever possible, the predictions have been compared with the experimental data reported in the literature. In what follows, the details on the specification of material functions are discussed first; later, the results of the numerical simulations are presented.

4.2.1 Specification of Material Functions

The inelastic deformation process has been described by invoking the framework presented in section 4.1.2. The yield condition on an arbitrary plane with unit normal n_i, equation (4.3), has been defined in a functional form similar to that of the failure criterion, equation (4.1). Thus, in the compression regime, a linear approximation has been employed

$$f(n_i)=\tau+\eta(\sigma-\sigma_o^c)=0; \qquad \eta=\eta(\kappa) \tag{4.16}$$

where $\sigma_o^c = \sigma_o \mu^t / \mu^c$ and κ is a hardening parameter. The hardening effects have been attributed here to the plastic shear strain, i.e.

$$\eta = \mu^c \frac{\kappa}{A+\kappa}; \quad \kappa = \int \dot{\gamma}^p dt \tag{4.17}$$

where $\dot{\gamma}^p = \dot{\bar{e}}_1^p$ and A is a material constant. It should be noted that, according to equation (4.17), as $\kappa \to \infty$ there is $\eta \to \mu^c$ which implies that $f(n_i) \to F(n_i)$. Thus, the conditions at failure are consistent with those stipulated by equation (4.1).

The plastic flow has been described by a non-associated rule, equation (4.4), in which the potential function has been defined as

$$\psi(n_i) = \tau - \eta_c (\sigma - \sigma_o^c) \ln \frac{\sigma_o^c - \sigma}{\hat{\sigma}_o} = 0 \tag{4.18}$$

Here, η_c is a parameter which represents the value of $\eta = \tau / (\sigma_o^c - \sigma)$ at which a transition from compaction to dilatancy takes place. Given the above formulation, the constitutive relation, equation (4.8), can now be established following the standard plasticity formalism. The consistency condition $\dot{f}(n_i) = 0$ reads

$$\frac{\partial f}{\partial \bar{t}_i} \dot{\bar{t}}_i + \frac{\partial f}{\partial \eta} \frac{\partial \eta}{\partial \kappa} \dot{\bar{e}}_1^p = 0 \tag{4.19}$$

where, according to equation (4.4)

$$\dot{\bar{e}}_1^p = \dot{\lambda}\frac{\partial \psi}{\partial \tau}; \qquad \frac{\partial \psi}{\partial \tau} = 1 \tag{4.20}$$

Thus, substituting (4.20) in (4.19) yields

$$\dot{\lambda} = \frac{1}{H}\frac{\partial f}{\partial \bar{t}_i}\dot{\bar{t}}_i; \qquad H = -\frac{\partial f}{\partial \eta}\frac{\partial \eta}{\partial \kappa} \tag{4.21}$$

where, H represents the plastic hardening modulus. Noting now that

$$\dot{\bar{t}}_i = T_{ji}\dot{t}_j; \qquad \dot{t}_i = \dot{\sigma}_{ij}n_j \tag{4.22}$$

equation (4.21) can be expressed in the form

$$\dot{\lambda} = \frac{1}{H}\frac{\partial f}{\partial \bar{t}_i}T_{ji}\dot{\sigma}_{jk}n_k \tag{4.23}$$

Finally, substituting equation (4.23) into equation (4.8), results in the following constitutive relation

$$\dot{\varepsilon}_{ij} = \left(C_{ijkl} + \frac{1}{8\pi}\int_S \frac{1}{H}\frac{\partial \psi}{\partial \bar{t}_p}\frac{\partial f}{\partial \bar{t}_q}(T_{ip}T_{kq}\,n_j\,n_l + T_{jp}T_{kq}\,n_i\,n_l)\;dS \right)\dot{\sigma}_{kl} \tag{4.24}$$

where, according to (4.16) - (4.18)

$$\frac{\partial f}{\partial \tau}=1\,;\quad \frac{\partial f}{\partial \sigma}=\eta\,;\quad \frac{\partial \psi}{\partial \tau}=1\,;\quad \frac{\partial \psi}{\partial \sigma}=\eta-\eta_c$$
$$\frac{\partial f}{\partial \eta}=\sigma-\sigma_o^c=-\frac{\tau}{\eta};\quad \frac{\partial \eta}{\partial \kappa}=\mu^c\frac{A}{(A+\kappa)^2} \tag{4.25}$$

In the tension regime, the hardening effects have been neglected, i.e. the behaviour was assumed to be elastic prior to the onset of localized deformation. It should be noted that in order to maintain a smooth transition between the compression and tension regimes, the hardening parameter, as specified in equation (4.17), needs to be re-defined. Thus, one can introduce a more general form

$$\dot{\kappa}=\dot{\gamma}^p/\phi;\qquad \phi=\phi(\sigma) \tag{4.26}$$

Here, the function ϕ should satisfy $\phi(0)\to 0$, and may be chosen such that $\sigma\to-\sigma_o\Rightarrow\phi\to 1$.

Finally, it is noted that the elastic properties associated with each sampling plane can be defined by invoking the dyadic decomposition in equation (4.5). Thus,

$$t_i=\sigma_{ij}\,n_j=A_{ij}\,e_j\,;\qquad A_{ij}=D_{ijkl}\,n_j\,n_k \tag{4.27}$$

where $D_{ijkl}=C_{ijkl}^{-1}$ is the elastic stiffness operator, which has been estimated here based on a homogenization procedure described in Pietruszczak & Niu (1992).

The strain localizes on a 'critical' plane, for which the value of the failure function $F(n_i)$ is maximum. The description of the localized deformation requires the specification of the operator K_{ij}, equation (4.12), which defines the properties of the material confined to the fracture zone. These properties have been described here by invoking a simple plasticity framework, which incorporates a strain-softening. In particular, the yield criterion in compression/tension domain was assumed in a functional form consistent with representation (4.1), i.e.

$$f(n_i)=\tau+\mu\sigma-\mu^t\bar{\sigma}_o=0 \qquad (4.28)$$

where n_i specifies now the normal to the localization plane, $\bar{\sigma}_o$ is the softening function and $\mu=const.$ is evaluated at the inception of localization. Note that in tension regime, $\mu=\mu^t$, whereas in compression $\mu\to\mu^c$.

The strain-softening effects have been attributed to the normal component of the velocity discontinuity g_2^p and the degradation function $\bar{\sigma}_o=\bar{\sigma}_o(\kappa)$ has been selected in a simple exponential form

$$\bar{\sigma}_o=\sigma_o e^{-C\kappa}; \qquad \kappa=\int\dot{g}_2^p dt \qquad (4.29)$$

where σ_o is the tensile strength in the direction normal to the localization plane and C represents a material constant. The formulation incorporated an associated flow rule, which in the context of equation (4.28), resulted in a progressive dilation in the fractured zone.

Given equations (4.28) and (4.29), the operator K_{ij} can now be established following once again the standard plasticity procedure. Introducing a local frame $\bar{x}$ associated with the base vectors n_i and s_i, where $n_i s_i = 0$, and assuming additivity postulate between the elastic and plastic strain increments, the generalized Hooke's law can be written as

$$\dot{\bar{g}}_i - \dot{\bar{g}}_i^p = \bar{C}_{ij}^e \, \dot{\bar{t}}_j \tag{4.30}$$

In the expression above $\bar{g}_i = \{\bar{g}_1, \bar{g}_2, 0\}$, $\bar{t}_i = \{\tau, \sigma, 0\}$, and

$$\bar{C}_{ij}^e = \begin{bmatrix} 1/K_T & 0 & 0 \\ 0 & 1/K_N & 0 \\ 0 & 0 & 1/K_T \end{bmatrix} \tag{4.31}$$

where, K_T and K_N represent the shear and normal stiffness, respectively, which can be formally derived from conventional elastic constants E and ν as

$$K_T = \frac{E}{2t(1+\nu)}; \quad K_N = \frac{E(1-\nu)}{t(1+\nu)(1-2\nu)} \tag{4.32}$$

Assuming now the associated flow rule, we have

$$\dot{\bar{g}}_i^p = \dot{\lambda} \frac{\partial f}{\partial \bar{t}_i} \tag{4.33}$$

where $\dot{\lambda}$ is a positive proportionality constant. The consistency condition $\dot{f} = 0$ reads

$$\frac{\partial f}{\partial \bar{t}_i} \dot{\bar{t}}_i + \frac{\partial f}{\partial \bar{\sigma}_o} \frac{\partial \bar{\sigma}_o}{\partial \bar{g}_2^p} \dot{\bar{g}}_2^p = 0 \tag{4.34}$$

which, in view of equation (4.33), reduces to

$$\frac{\partial f}{\partial \bar{t}_i}\dot{\bar{t}}_i + \frac{\partial f}{\partial \bar{\sigma}_o}\frac{\partial \bar{\sigma}_o}{\partial \bar{g}_2^p}\dot{\lambda}\frac{\partial f}{\partial \sigma} = 0 \tag{4.35}$$

Thus,

$$\dot{\lambda} = \frac{1}{H}\frac{\partial f}{\partial \bar{t}_i}\dot{\bar{t}}_i \tag{4.36}$$

where

$$H = -\frac{\partial f}{\partial \bar{\sigma}_o}\frac{\partial \bar{\sigma}_o}{\partial \bar{g}_2^p}\frac{\partial f}{\partial \sigma} \tag{4.37}$$

and H denotes the plastic softening modulus. Combining equations (4.30), (4.33), and (4.36), we have

$$\dot{\bar{g}}_i = \bar{K}_{ij}\dot{\bar{t}}_j \ ; \qquad \bar{K}_{ij} = \bar{C}_{ij}^e + \frac{1}{H}\frac{\partial f}{\partial \bar{t}_i}\frac{\partial f}{\partial \bar{t}_j} \tag{4.38}$$

which, in the context of representation (4.28), reduces to

$$\bar{K}_{ij} = \begin{bmatrix} 1/K_T & 0 & 0 \\ 0 & 1/K_N & 0 \\ 0 & 0 & 1/K_T \end{bmatrix} + \frac{1}{H_p}\begin{bmatrix} 1 & \mu & 0 \\ \mu & \mu^2 & 0 \\ 0 & 0 & 0 \end{bmatrix} \quad ; \qquad H_p = -C\,\mu\,\mu'\,\bar{\sigma}_o \tag{4.39}$$

The operator K_{ij} can now be established by invoking the standard transformation rule

$$K_{ij} = T_{im}T_{jn}\bar{K}_{mn} \tag{4.40}$$

where T_{ij} is the transformation matrix.

It should be mentioned here that, in order to ensure the sensitivity of the softening characteristics to the value of normal stress, the definition of parameter κ, equation (4.29), may be augmented in a manner similar to representation (4.26).

Finally, note that after the inception of strain localization, the material response is sensitive to the 'characteristic dimension' υ, which appears in the constitutive relation (4.15). In the numerical simulations carried out in this work, the value of υ was estimated by assuming that the representative volume, V, is enclosed by a sphere with the radius $R = \sqrt[3]{3V/4\pi}$. In this case, the characteristic dimension υ can be approximated as $\upsilon = 3/4R$.

4.2.2 Numerical Results

The formulation of the problem, as presented above, incorporates a number of material parameters which need to be identified. Those include, in addition to elastic constants, a set of parameters defining the conditions at failure, i.e. those appearing in the distribution functions (2.14); the parameters A and η_c, equations (4.17)-(4.18), governing the inelastic behaviour on the i-th plane; and the parameter C, equation (4.29), specifying the rate of softening associated with the localized deformation.

The distribution functions (2.14) were selected based on the experimental data reported by Page (1983). The details on the identification procedure have been provided in section 2.3.1. The corresponding values are:

$\mu_o^t = 2.4;\ \mu_o^c = 1.1;\ \sigma_{01} = 0.88MPa;\ \sigma_{02} = -5.34MPa;\ \sigma_{03} = 0.60MPa;$
$\Omega_1^{\mu^t} = 0.06;\ \Omega_1^{\mu^c} = 0;\ \Omega_1^{\sigma_o} = -0.226$

The elastic properties of the brickwork can, in general, be estimated by invoking a homogenization procedure. In the numerical simulations presented here, the values of elastic constants have been chosen based on the estimates developed in the article by Pietruszczak & Niu (1992). Using the properties of constituents and the geometric arrangement similar to those reported by Page, the following values have been selected:

$E_1 = 7,700MPa;\ E_2 = 8,800MPa;\ \nu_{13} = 0.25;\ \nu_{21} = 0.29;\ G_{12} = 1,760MPa$

The results reported by Page provide no information on the stress-strain characteristics. Therefore, the values of the parameters governing the inelastic response have been estimated from other sources. The hardening parameter A has been chosen through a trial and error procedure, by examining the numerical predictions for a set of axial compression tests at different orientations of the bed joints, as reported by Drysdale & Khattab (1995). The results indicate that the axial strain at failure, in the direction of loading, is in the range of 0.1%. By adopting this as a guideline, the value of A was estimated to be in the range of A=0.00005. It should be noted that, given the appropriate experimental data, the parameter A may also be defined in terms of a distribution function similar to that employed in equation (2.14). Furthermore, the transition from compaction to dilatancy was assumed to occur at $\eta_c = 0.95\mu^c$, which is typical for a broad class of brittle-plastic materials (e.g. Kupfer et al., 1969; Kotsovos & Newman, 1979). Finally, no information is currently available pertaining to specification of the softening parameter C, equation (4.29). Therefore, some parametric studies have been conducted examining the sensitivity of the global characteristics to the value of this parameter.

The first set of numerical results, as shown in Figures 4.2 and 4.3, pertains to specification of conditions at failure in a series of axial compression/tension tests, performed at different orientation of bed joints relative to the loading direction. Figure 4.2a shows the distribution of compressive strength, whereas figure 4.2b presents the corresponding evolution of the orientation of the localization plane. The results based on the proposed formulation are compared here with the experimental data of Page (1983) as well as with an exact solution obtained by solving a constrained optimization problem (see section 2.2). The primary objective here is to investigate the accuracy of different integration schemes employed in equation (4.7). The results for the multi-laminate model correspond to a 2D sampling rule incorporating a set of 36 uniformly distributed planes. It is evident that this integration scheme is sufficiently accurate. A similar conclusion can be drawn based on the results reported in figure 4.3, which pertain to a set of axial tension tests.

A detailed discussion on the basic trends in the material response, as depicted in figures 4.2 and 4.3, has been given in section 2.3.2. It is evident again that for low values of β the failure occurs through formation of macrocracks in the masonry units, in the direction which is in a close proximity of head joints. At $\beta \approx 40^0$ there is a transition in the failure mode, i.e. the localization plane is shifted to the region in the vicinity of the bed joints. A somewhat similar trend can be observed in tension, figure 4.3b. Here, for $\beta \leq 30^0$, the failure of the brickwork is induced by rapture of the head joints, whereas for $\beta > 40^0$, the failure occurs in the bed joints.

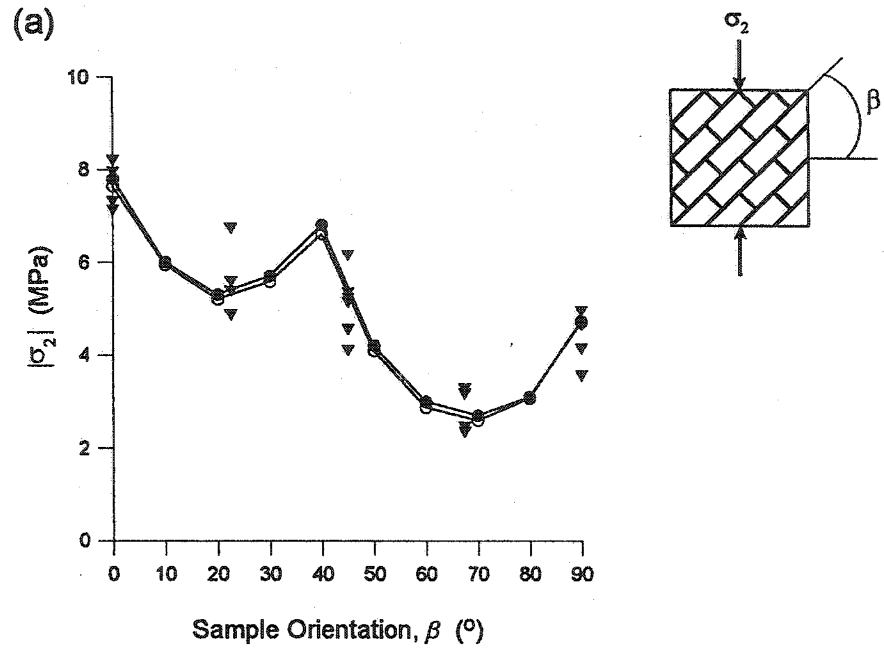

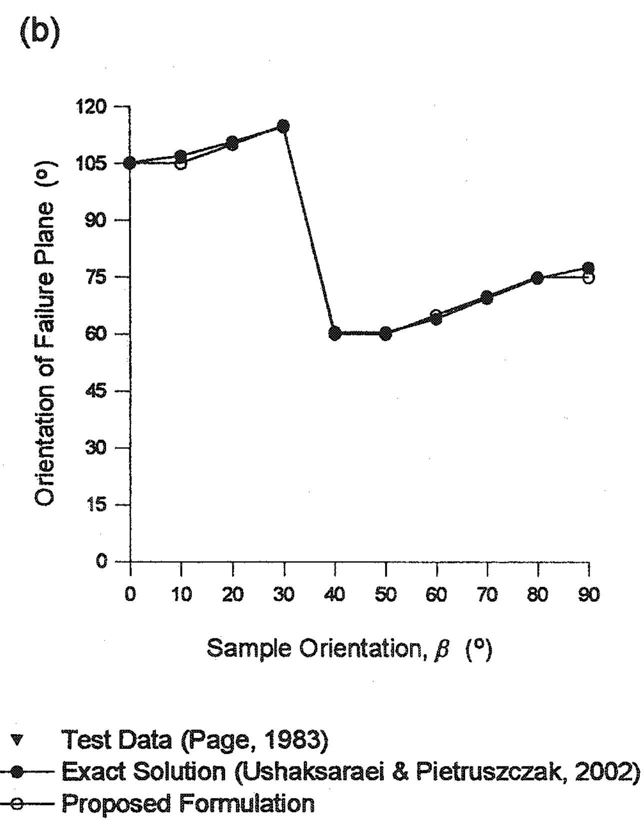

Figure 4.2 Variation of uniaxial compressive strength and orientation of failure plane with sample orientation.

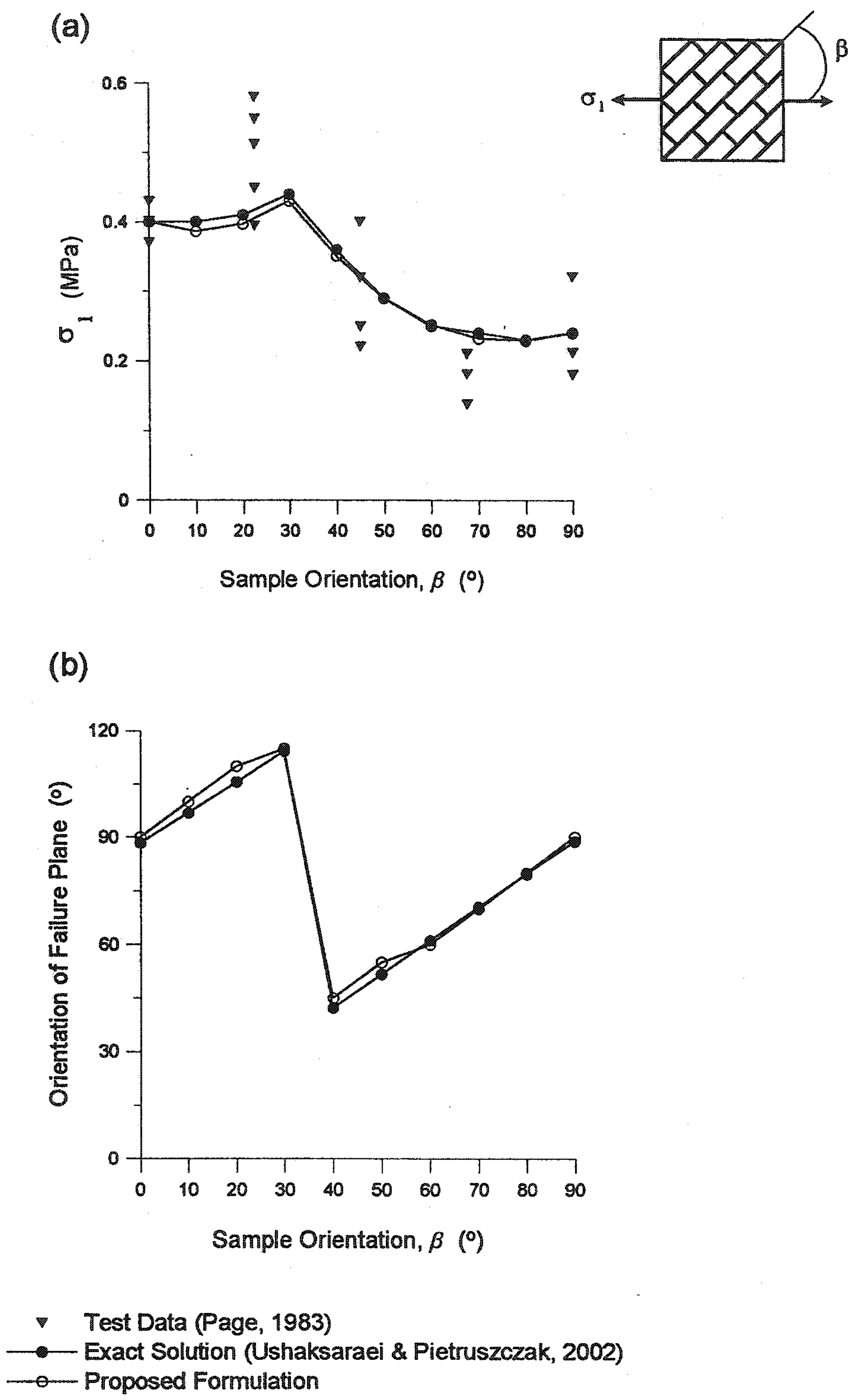

Figure 4.3 Variation of uniaxial tensile strength and orientation of failure plane with sample orientation.

Complete mechanical characteristics corresponding to compression regime are shown in a set of subsequent figures. Figure 4.4 presents the stress-strain response in uniaxial compression for different orientations of the bed joints. The characteristics shown here include the descending branches, associated with the localized deformation mode. The latter have been computed assuming that the transition to localized mode commences at $\mu = 0.99\mu^c$, while C=60m^{-1}, equation (4.29), and V=0.03m^3. The influence of the last two parameters on the mechanical response is investigated further in figure 4.5. Here, the simulations are performed for β=0^0. Evidently, an increase in the value of C results in a steeper descending branch. It is also apparent that the response in the post-localized regime is sensitive to the geometry of the sample. For the same value of C, the average rate of strain-softening increases with the size of the sample.

Figure 4.6 presents the variation of vertical compressive stress, in the hardening regime, with both the axial and lateral strains. The trends, as depicted in this figure, are fairly consistent with the experimental data reported by Drysdale & Khattab (1995). For all tests considered here, the deformation mode is, in general, anisotropic; i.e. the change in vertical stress is accompanied by distortion of the sample. This is evidenced in figure 4.7, which presents the evolution of shear strain in samples tested at different orientation relative to the loading direction.

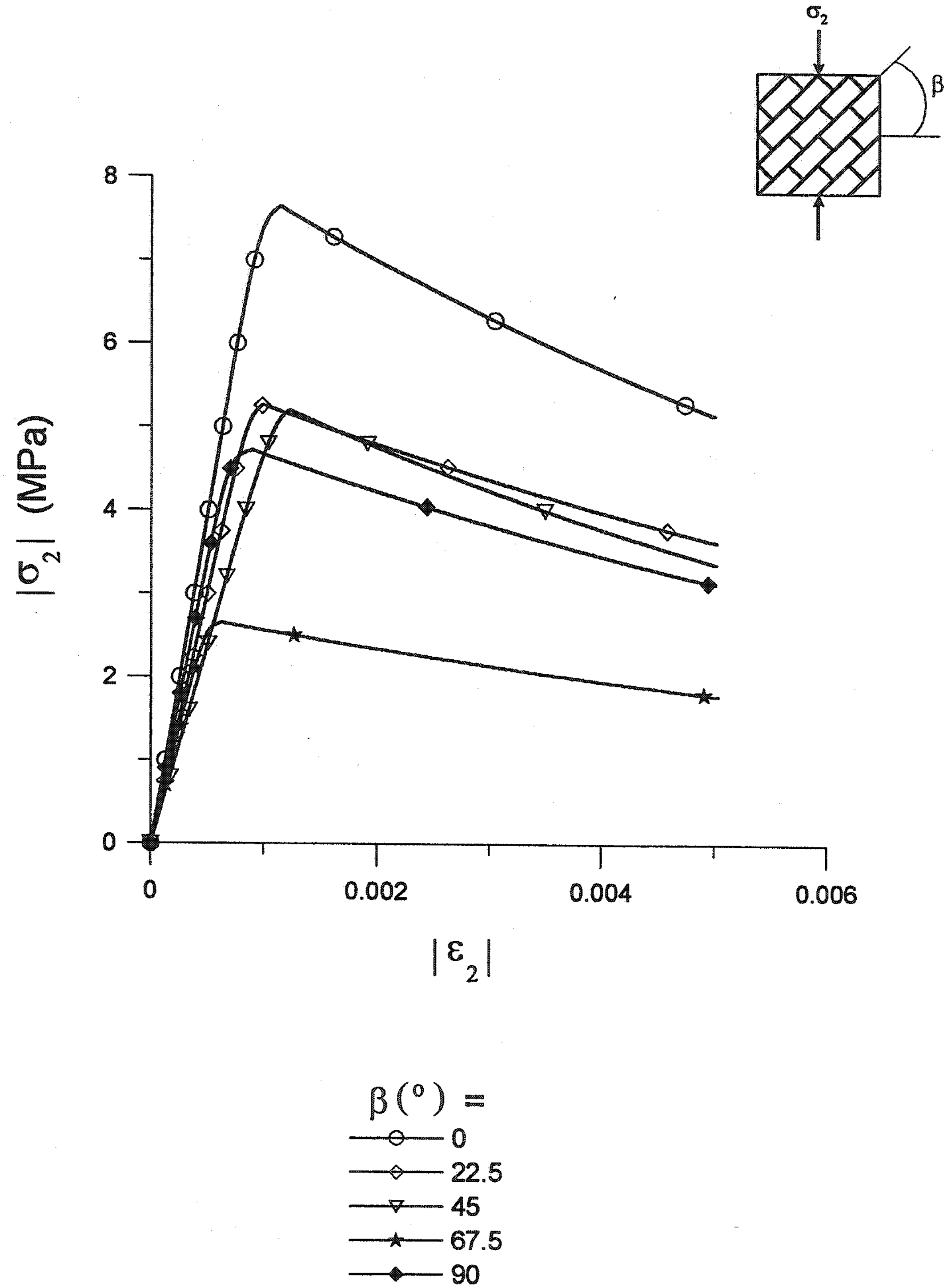

Figure 4.4 Stress-strain response in uniaxial compression for different orientations of bed joints.

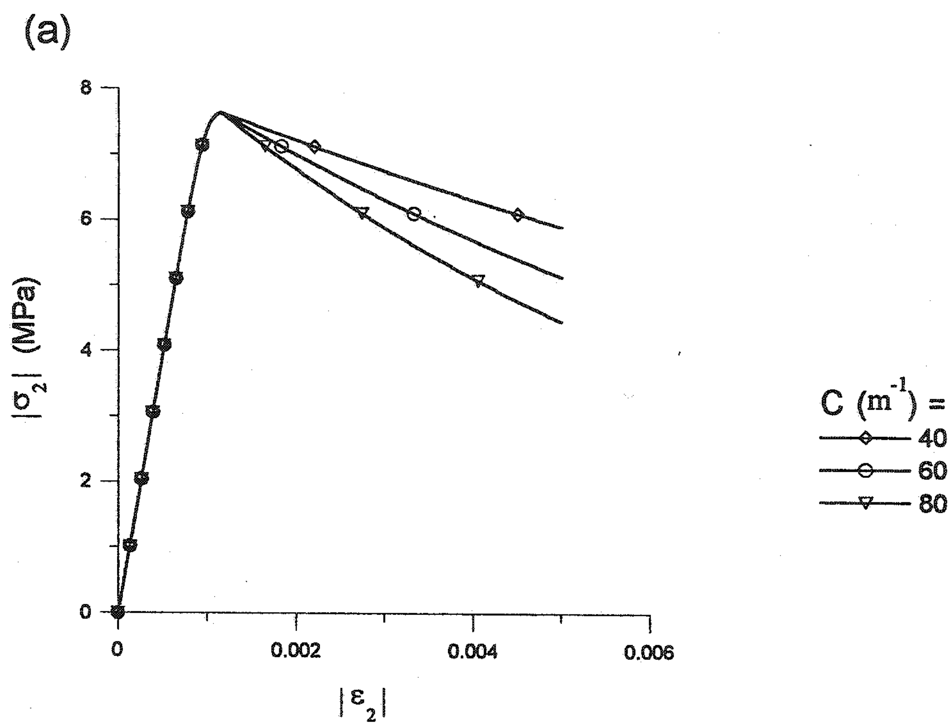

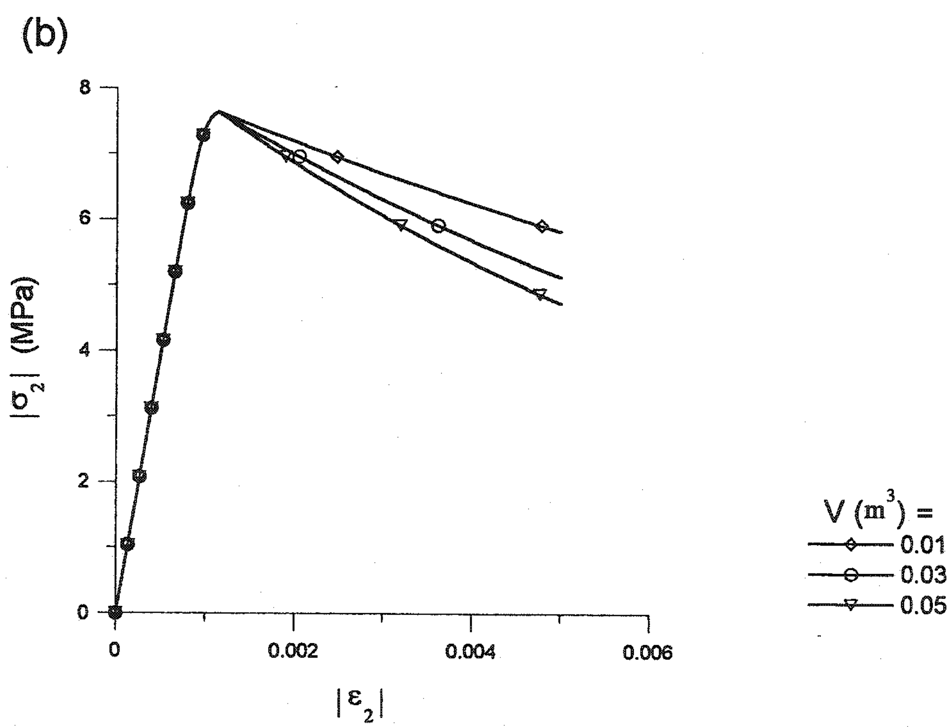

Figure 4.5 Influence of the softening parameter, C, and the volume of the sample, V, on the response in uniaxial compression (β=0°).

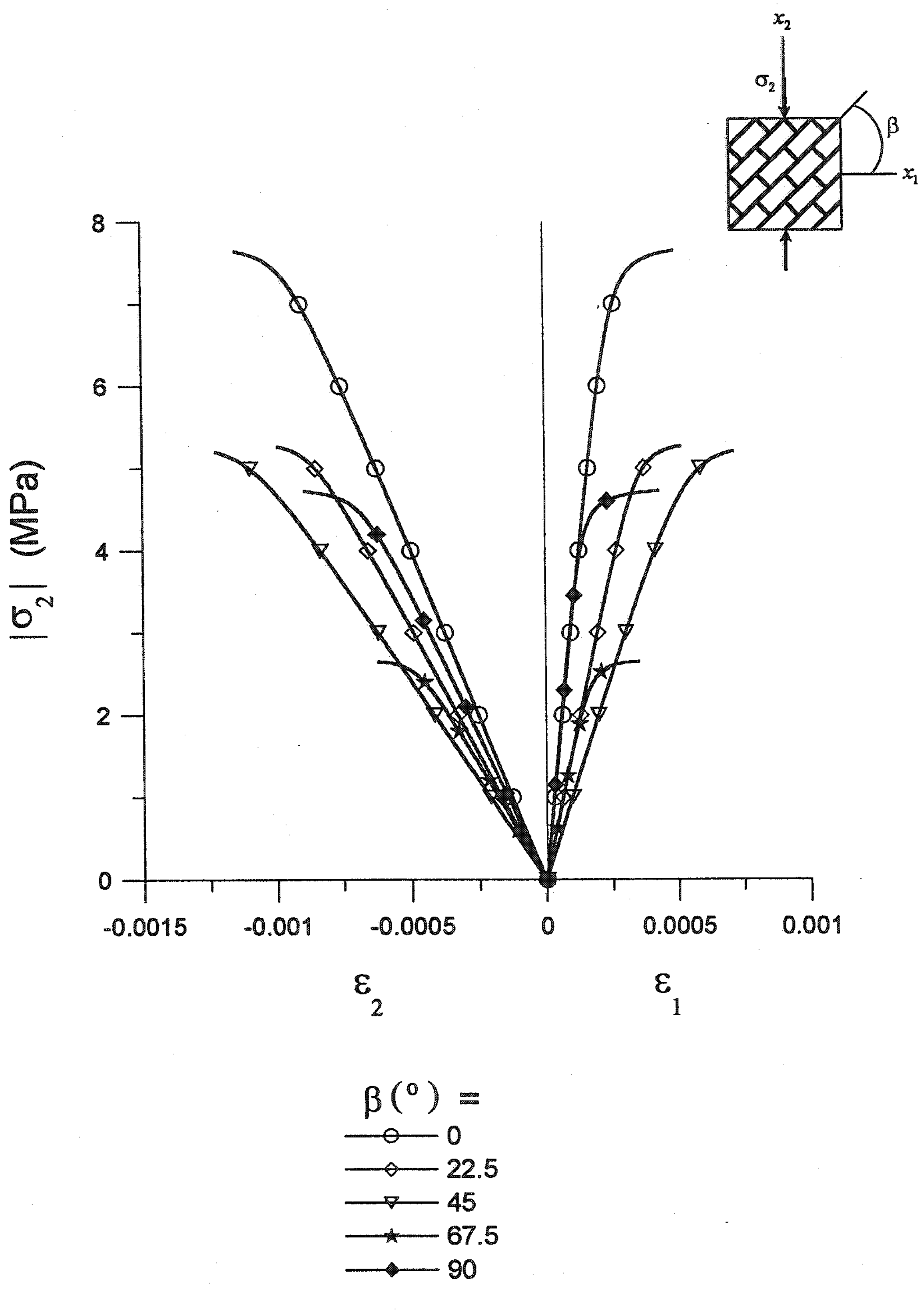

Figure 4.6 Stress-strain characteristics in uniaxial compression (in hardening regime).

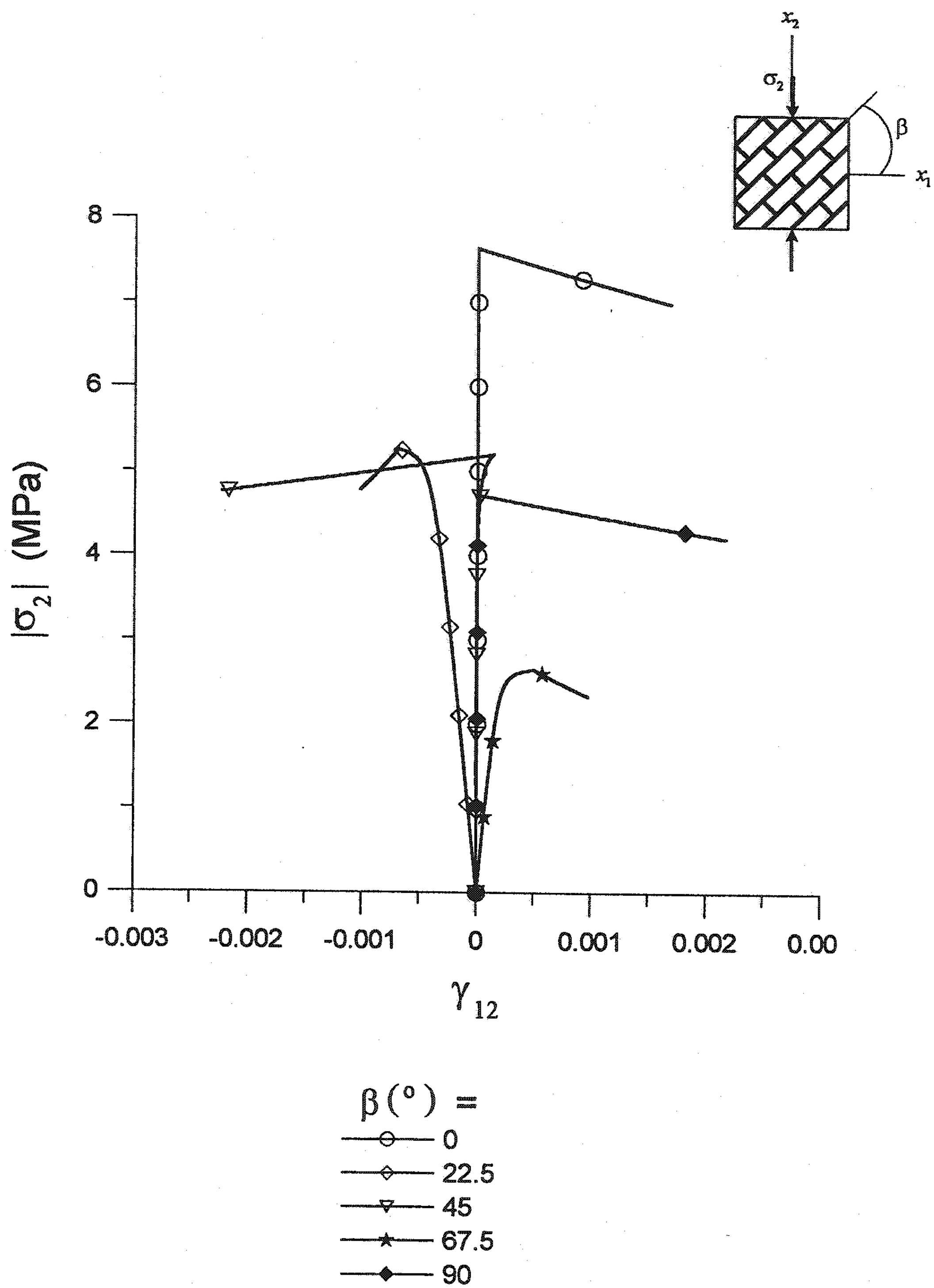

Figure 4.7 Evolution of shear strain in uniaxial compression tests.

4.3 Inelastic F.E. Analysis of a Bearing Masonry Wall Subjected to In-Plane Loading

The proposed constitutive model has been implemented in a finite element code. In what follows, a heuristic example is provided involving a brick masonry wall subjected to in-plane loading. The primary objective here is to investigate the evolution of the cracking pattern leading to the collapse of the wall, and to examine a simple reinforcement strategy.

The wall, 25 m in width,10 m high, and 0.20 m thick, is assumed to be made of unreinforced masonry and has three identical openings with a symmetric arrangement with respect to the centre-line. The loading process consists of applying uniform vertical displacements along the upper surface under the condition of perfect bonding at the base. Owing to the symmetry in geometry and boundary conditions only a half of the structure was analysed, assuming no horizontal movement along the centre-line of the wall. The wall was discretized using four-noded rectangular elements, as depicted in figure 4.8, with isoparametric formulation and 2×2 Gauss quadrature. The material parameters selected for the analysis were identical to those used for the numerical simulations discussed in the preceding section. The characteristic dimension υ was identified based on the volume associated with each Gauss point. The problem was solved using the 'tangential stiffness' approach (Owen & Hinton, 1980) and employing a non-symmetric equation solver. Since the analysis incorporating the homogenization procedure, equation (4.15), shows little sensitivity to the discretazation, no explicit mesh convergence study was performed.

The results of the numerical simulations are shown in figures 4.9-4.11. Figure 4.9 presents the global load-displacement characteristic for the wall. The ultimate conditions are reached at the external load of about 25 MN, after which the response becomes unstable. Figure 4.10 shows the distorted mesh at the stage preceding the collapse of the wall. It is evident here that significant distortions develop in the neighbourhood of the openings. Figure 4.11 shows the evolution of the crack pattern in tension and compression regimes. At the early stages of the deformation process, the tensile cracks form in the region adjacent to the openings and propagate upwards, figure 4.11a. As the load increases further, some compressive cracks develop along the vertical boundaries nearby the openings. Figure 4.11b presents the distribution of the damage zones at the ultimate load.

In order to improve the stability of the wall, a simple reinforcement scenario has been considered. This involved reinforcing the window frames with steel braces and placing above the openings a continuous horizontal beam, incorporating W360x122 cross-section. The results of numerical simulations are shown in figure 4.12. Figure 4.12a presents the load-displacement characteristic, whereas figure 4.12b depicts the pattern of cracking at the external load of about 25 MN (i.e. the ultimate load for the unreinforced system). It is evident that a simple reinforcement strategy employed here is quite efficient. The extent of structural damage is significantly less pronounced and the global characteristic remains in the linear range. For the case considered here, the collapse is associated with yielding of the reinforcement and takes place at much higher load intensities.

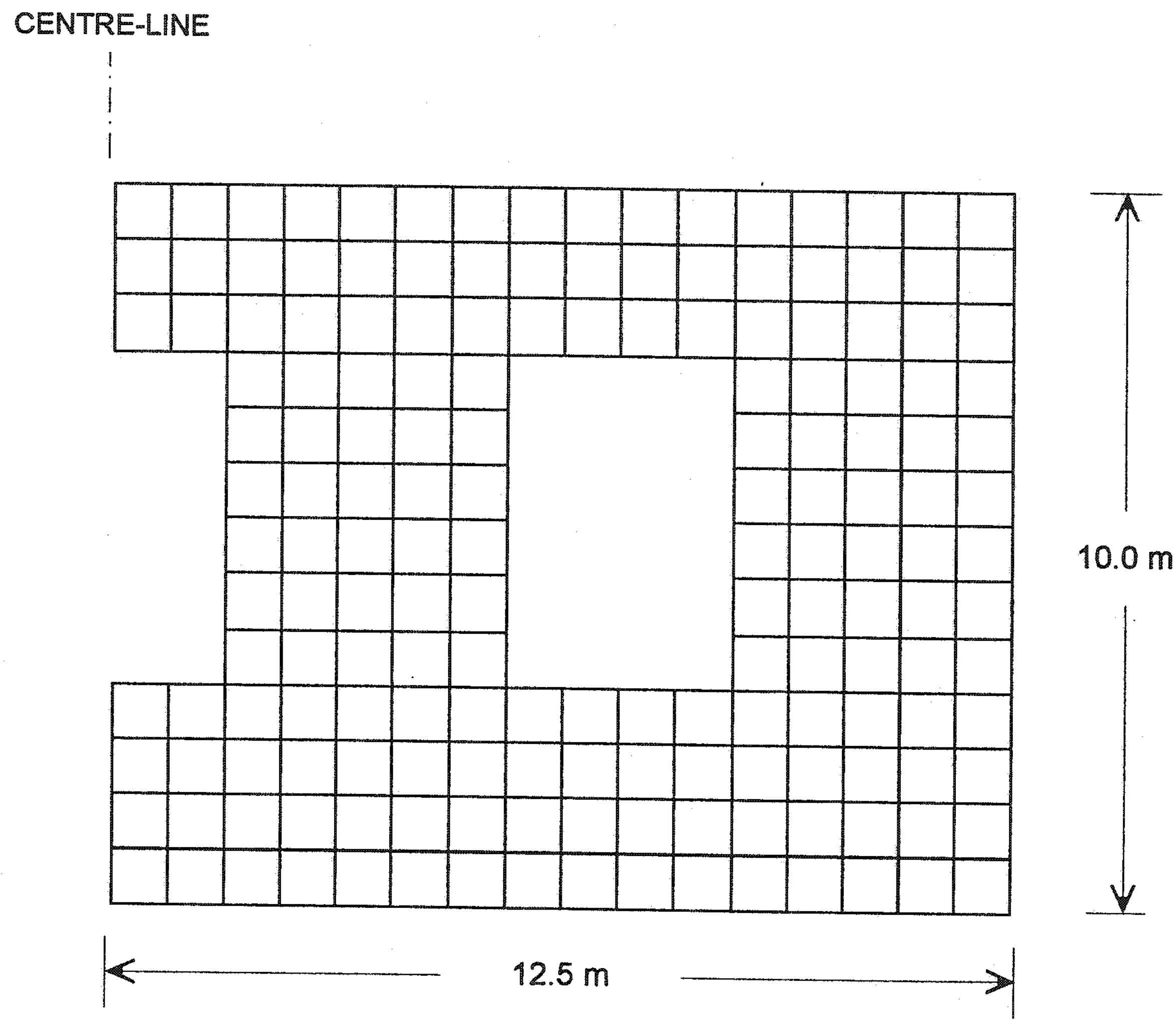

Figure 4.8 Finite element discretization of the unreinforced masonry wall.

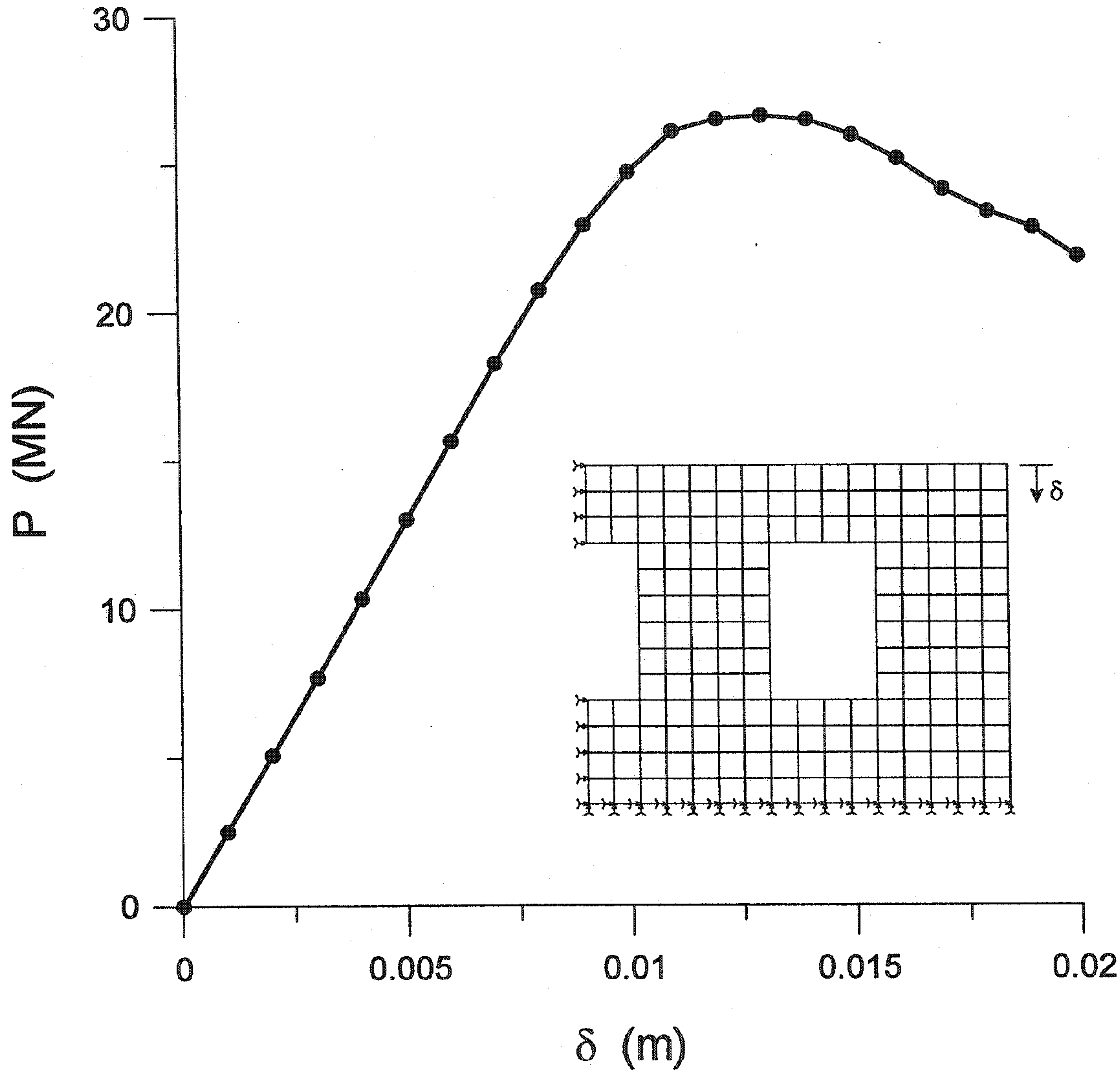

Figure 4.9 Global load-displacement response of the unreinforced bearing wall.

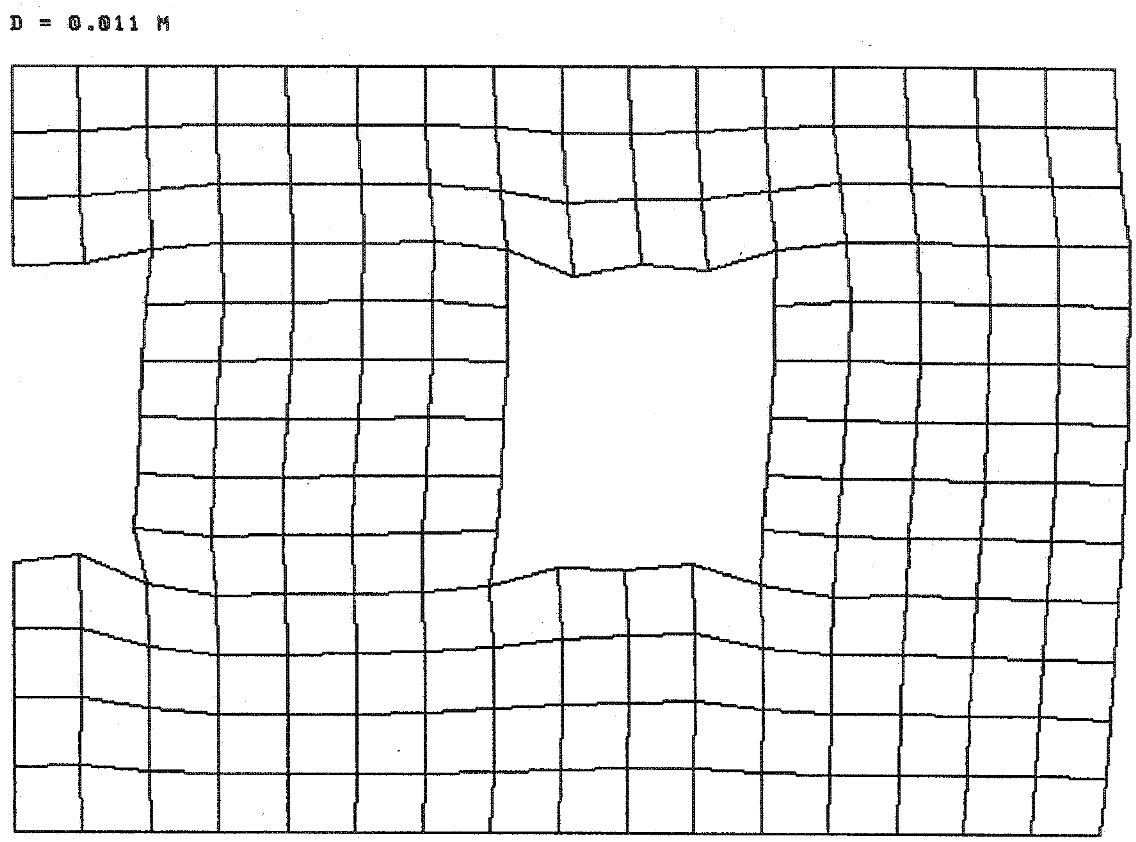

Figure 4.10 Distorted mesh of the unreinforced wall at the ultimate load.

(a)

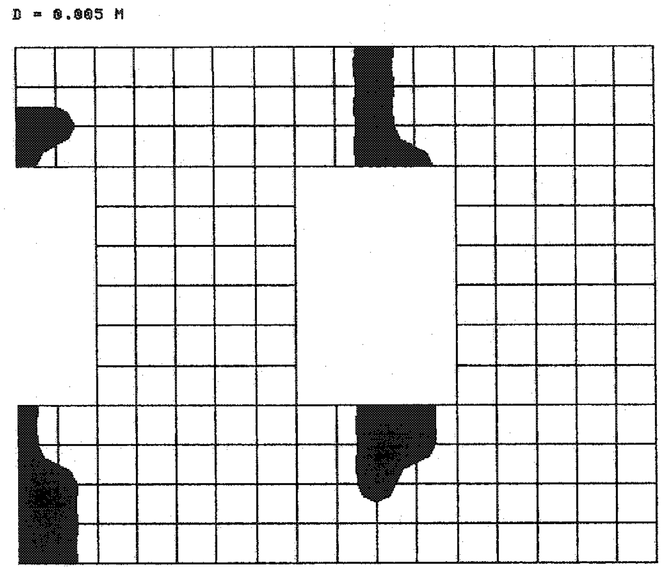

(b)

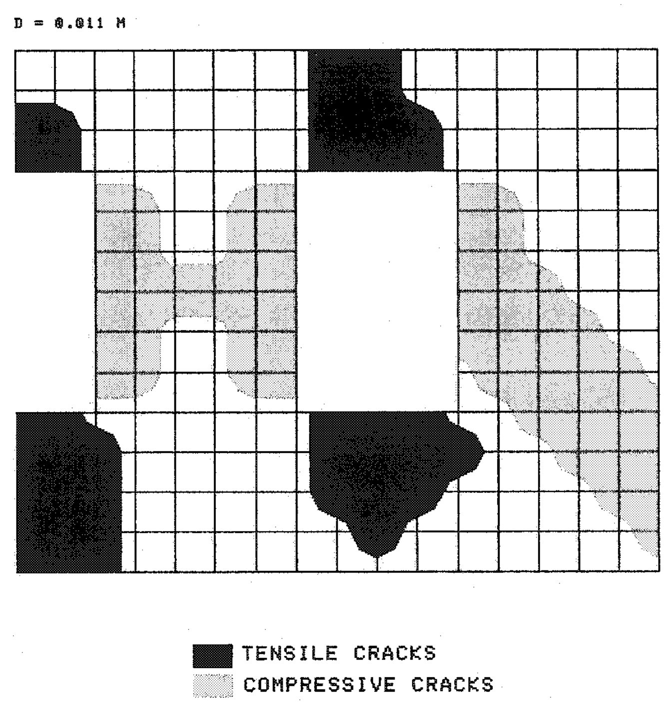

Figure 4.11 Evolution of crack patterns in tension and compression regimes for the unreinforced bearing wall.

(a)

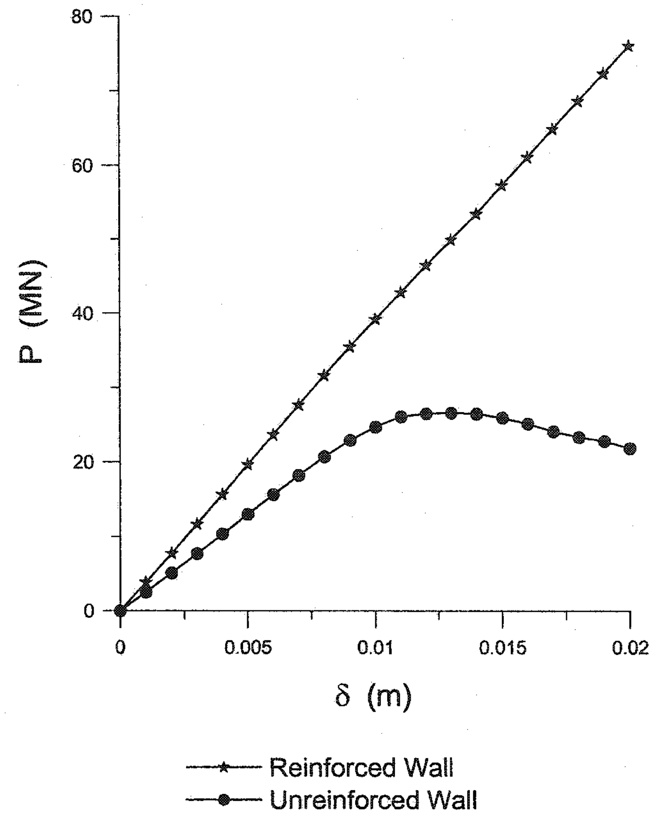

(b)

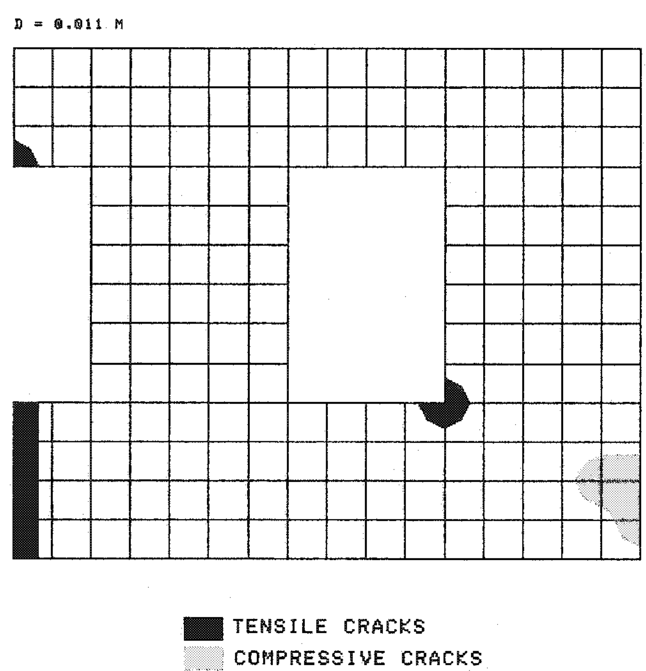

Figure 4.12 (a) Global load-displacement response of the reinforced bearing wall and (b) crack patterns at the ultimate load.

CHAPTER 5

CONCLUSIONS AND RECOMMENDATIONS

In this chapter, a summary of the major conclusions from the preceding chapters is presented. Particularly, the highlights of the two main aspects of the research are discussed:

1) a macroscopic failure criterion for structural masonry based on the critical plane approach

2) a constitutive law for the description of the inelastic response of the material and its implementation in a nonlinear finite element analysis

Subsequently, recommendations for future work resulting from the research are discussed. The thesis concludes with some final remarks on the modelling of the nonlinear behaviour of the structural masonry.

5.1 Summary and Conclusions

The specification of the conditions at failure for structural masonry constitutes an important problem. In chapter 1, it was pointed out that the standard approach based on homogenization techniques was complex in numerical implementation and was bound to incorporate several simplifying assumptions pertaining to kinematics of the constituents. Furthermore, it was shown that there was no constitutive law suitable for implementation in a finite element code to simulate the nonlinear behaviour of the structural masonry. In other words, the formulation that incorporates the anisotropic material characteristics and addresses all stages of the deformation process is not available in the literature.

In chapter 2, an approach was developed aimed at the specification of a macroscopic failure criterion which would account for the structural arrangement of the brickwork. The formulation was derived within the framework of the critical plane approach as proposed by Pietruszczak and Mroz (2001). The approach incorporated a set of distribution functions for describing the spatial variation of material properties. The orientation of the localization plane was defined as a constrained optimization problem. Based on the general theory, an extension of the critical plane framework was proposed for the case of a nonlinear failure function, which was more suitable for the class of brittle materials. Subsequently, the macroscopic failure criterion for structural masonry was introduced, which incorporated a bilinear approximation to the quadratic form employed earlier. The advantage of this approximation is twofold. First, the equations governing the conditions for a stationary value of the Lagrangian function, are algebraically more simple. Second, the bi-linear form allows one to decouple the problem of identification of the distribution functions, i.e., $\mu^t(n_i)$ and $\mu^c(n_i)$ can be specified independently from tests in tension and compression regimes, respectively.

The material parameters/functions were identified from the experimental data reported by Page (1983). Several other authors have also conducted similar tests on masonry panels (e.g., Samarasinghe and Hendry, 1982; Drysdale and Khattab, 1995). In general, regardless of which particular set of experimental data is used, the information is not adequate to identify all constants involved and some intuitive assumptions had to be made. At the same time, the results reported by Page are still the most comprehensive source of the data available to date. They include a significant number of loading histories for a broad range of orientations of bed joints, and provide explicit information on the corresponding failure mode.

The verification of performance of the proposed approach involved a study on the sensitivity of the conditions at failure to the orientation of bed joints for a number of biaxial tension/compression loading histories. It was demonstrated that the predicted trends were fairly consistent with the experimental evidence. Furthermore, it was pointed out that for the in-plane loading, the out-of-plane properties might play a significant role in defining the conditions at failure. This was particularly relevant to compression-compression regime, which generally required the assumption of orthotropy. A significant advantage of the approach advocated here over other possible continuum approximations lies in the fact that the orientation of the localization plane can be uniquely predicted. This is of particular importance in defining the response in the post-localization regime.

The structural effects of seismic loading on buildings constructed with unreinforced masonry bearing walls are frequently misinterpreted, and the proposed upgrading interventions can not be always justified. The decisions regarding various types of refurbishing methods to reinforce these types of structures in order to satisfy the requirements of the latest building codes, are often intuitive or based on inadequate methodologies. In this context, the primary objective of chapter 3 was to outline a simple and rational approach for assessing the effects of seismic load on masonry structures. While the quantitative aspects require further experimental verification, it is evident that the proposed methodology can be quite effective in examining various reinforcement strategies.

In chapter 4, the focus was on the description of progressive failure in structural masonry. In this context, a continuum formulation was developed to simulate the inelastic behaviour of the structural masonry (Pietruszczak and Ushaksaraei, 2002). This seemed to be the first attempt to model the evolution of progressive failure in masonry structures. The formulation incorporated the anisotropic material characteristics and addressed both stages of the deformation process, i.e. those associated with homogeneous as well as localized deformation mode.

The proposed approach depicted the basic trends in the behaviour of structural masonry, in both tension and compression regimes, as evidenced in section 4.2. These include a strong sensitivity of mechanical characteristics to the orientation of the sample and the associated evolution of the direction of localization plane. The formulation may be perceived as a pragmatic alternative to the homogenization method. In fact, in the absence of appropriate experimental tests (which are expensive and difficult to perform), the homogenization approach may be implemented to generate a set of data, which can subsequently be used to identify the material parameters/functions involved. Such a methodology, in the context of the specification of the conditions at failure, was employed in Gocevski & Pietruszczak (2001). In section 4.3, the proposed model was successfully implemented in a nonlinear finite element analysis. The results provided an insight into the physical behaviour of the structure during the process of the progressive failure. Finally, the same formulation has also been applied to assess the efficiency of different reinforcement strategies.

5.2 Recommendations for Future Work

In the present research, some fundamental aspects of the behaviour of the structural masonry have been addressed. Although the results are quite reasonable and promising, further research is still required to improve the performance of the proposed models. In what follows, some recommendations for future research are presented based on the present study.

Some supplementary experimental studies are required to identify the material parameters more accurately. For example, some direct shear tests in both tension and compression regimes may be required to identify the failure function proposed in chapter 2. Furthermore, for the biaxial compression tests, the identification of the parameters based on the in-plane test data available in the literature is not sufficiently accurate and the results of the numerical simulations are not in a good agreement with the experimental data. Thus, for this particular loading history, further 3D tests are required. Also, in the context of the continuum model, some additional experimental information is needed to identify the hardening/softening parameters appearing in the formulation.

As mentioned in section 4.2, since the hardening effects in the tension regime are neglected, the relevant hardening function needs to be redefined to maintain a smooth transition between the compression and tension regimes. A similar improvement may be necessary in the definition of the softening function in the tension regime, in order to ensure the sensitivity of the softening characteristics to the value of the normal stress.

5.3 Final Remarks

The constitutive model proposed in this research incorporates the material anisotropy and describes all stages of the deformation process. It can be readily implemented in a finite element code to perform a nonlinear analysis to simulate the evolution of the progressive failure of the structural masonry. From a practical standpoint, the methodology developed here can be very useful in the context of the design of new masonry structures, the assessment of the stability of the existing structures, and also the investigation of the efficiency of different reinforcement strategies. The latter is of particular importance in the rehabilitation of existing unreinforced masonry structures.

REFERENCES

Anthoine, A. (1995). "Derivation of in-plane elastic characteristics of masonry through homogenization theory." *Int. J. Solids Struct.*, 32(2), 137-163.

Anthoine, A. (1997). "Homogenisation of periodic masonry: plane stress, generalized plane strain or 3D modelling?" *Commun. Numer. Methods Eng.*, 13, 319-326.

Baker, W. H. and Krizek, R. J. (1970). "Mohr-Coulomb strength theory for anisotropic soils." *J. Soil Mech. Found. Div., Am. Soc. Civ. Eng.*, 96(SM1), 269-292.

Casagrande, A. and Carrillo, N. (1944). "Shear failure of anisotropic materials." *J. Boston Soc. Civ. Eng.*, 31(4), 122-135.

Drysdale, R. G., and Khattab, M. M. (1995). "In- plane behavior of grouted concrete masonry under biaxial tension-compression." *ACI Struct. J.*, 92(6), 653-664.

Duveau, G., Shao, J. F. and Henry, J. P. (1998). "Assessment of some failure criteria for strongly anisotropic geomaterials." *Mech. Cohesive-Frict. Mater.*, 3, 1-26.

Gocevski, V., and Pietruszczak, S. (2001). "Seismic analysis of brick masonry walls of the Beauharnois powerhouse in Quebec, Canada." In: *Computer methods in structural masonry* –5. Computers & Geotechnics Ltd, pp.141-148.

Gocevski, V., Pietruszczak, S., and Ushaksaraei, R. (2002). "Seismic analysis of brick masonry walls of a power substation building." *Proc. Eighth Int. Symp. Numer. Models Geomech. - NUMOG VIII, Rome, Italy* (Edited by G. N. Pande and S. Pietruszczak), Balkema Publications, 643-648.

Hoek, E. (1968). "Brittle fracture of rock." *Rock Mechanics in Engineering Practice*, (Edited by K. G. Stagg and O. C. Zienkiewicz), John Wiley and Sons, London, England, 99-124.

Hoek, E. and Brown, E. T. (1980). "Empirical strength criterion for rock masses." *J. Geotech. Eng. Div., Am. Soc. Civ. Eng.*, 106(GT9), 1013-1035.

Jaeger, J. C. (1960). "Shear failure of anisotropic rocks." *Geol. Mag.*, 97(1), 65-72.

Kotsovos, M. D., and Newman, J. B. (1979). "A mathematical description of the deformation behaviour of concrete under complex loading." *Mag. Concr. Res.*, 31(107), 77-90.

Kupfer, H., Hilsdorf, H. K., and Rusch, H. (1969). "Behaviour of concrete under biaxial stress." *Proc. Am. Concr. Inst.*, 66(8), 656-666.

Lemos, J. V. (2001). "Modelling the behaviour of a stone masonry arch structure under cyclic loads." In: *Computer methods in structural masonry* –5. Computers & Geotechnics Ltd, pp.101-108.

Lourenco, P.B., and Zucchini, A. (2001). "A homogenization model for stretcher bond masonry." In: *Computer methods in structural masonry* –5. Computers & Geotechnics Ltd, pp.60-67.

Maier, G., Papa, E., and Nappi, A. (1991). "On damage and failure of unit masonry." *Experimental and numerical methods in earthquake engineering*, Balkema, Brussels, 223-245.

Masiani, R., and Trovalusci, P. (1996). "Cauchy and Cosserat materials as continuum models of brick masonry." *Meccanica*, 31, 421-432.

Owen, D. R. J., and Hinton, E. (1980). "Finite elements in plasticity: theory and practice." Pineridge Press, Swansea.

Page, A. W. (1981). "The biaxial compressive strength of brick masonry." *Proc. Inst. Civil Eng.*, 71(2), 893-906.

Page, A. W. (1983). "The strength of brick masonry under biaxial tension-compression." *Int. J. Masonry Constr.*, 3(1), 26-31.

Pande, G. and Lee, J. (1992). "A finite element homogenisation technique for bone and soft tissue interface analysis." *Proc. Recent Adv. Comp. Mech. Biomechanics and Biomedical Eng.*, 298-307.

Pande, G. N., Liang, J. X., and Middleton, J. (1989). "Equivalent elastic moduli for brick masonry." *Comput. Geotech.*, 8, 243-265.

Pande, G. N., and Sharma, K. G. (1983). "Multi-laminate model of clays -- a numerical evaluation of the influence of rotation of the principal stress axes." *Int. J. Numer. Analyt. Meth. Geomech.*, 7, 397-418.

Pietruszczak, S. (1999). "On homogeneous and localized deformation in water-infiltrated soils." *Int. J. Damage Mech.*, 8, 233-253.

Pietruszczak, S., and Mroz, Z. (2001). "On failure criteria for anisotropic cohesive-frictional materials." *Int. J. Numer. Analyt. Meth. Geomech.*, 25, 509-524.

Pietruszczak, S., and Niu, X. (1992). "A mathematical description of macroscopic behaviour of brick masonry." *Int. J. Solids Struct.*, 29(5), 531-546.

Pietruszczak, S., and Ushaksaraei, R. (2002). "Description of inelastic behaviour of structural masonry." *Int. J. Solids Struct.* (Submitted).

Samarasinghe, W. and Hendry, A. W. (1982). "Strength of brickwork under biaxial tensile and compressive stress." *Proc. Br. Ceram. Soc.*, 30, 129-139.

Sicilia, C., Pande, G. N., and Hughes, T.G. (2001). "Numerical modelling of masonry arch bridges." In: *Computer methods in structural masonry* –5. Computers & Geotechnics Ltd, pp.20-27.

Sulem, J., and Muhlhaus, H.B. (1997). "A continuum model for periodic two-dimensional block structures." *Mech. Coh. Frict. Mater.*, 2, 31-46.

Urbanski, A., Szarlinski, J., and Kordecki, Z. (1995). "Finite element modelling of the behaviour of masonry walls and columns by homogenization approach." In: *Computer methods in structural masonry* –3. B & J Intern., 32-41.

Ushaksaraei, R., and Pietruszczak, S. (2002). "Failure criterion for structural masonry based on critical plane approach." *J. Eng. Mech., Am. Soc. Civ. Eng.*, 128(7), 1-10.